2019

Quantifying the Performance of the Protodune Single Phase Neutrino Detector Using Computational Fluid Dynamics

Dillon Pedersen
South Dakota State University

QUANTIFYING THE PERFORMANCE OF THE PROTODUNE SINGLE PHASE NEUTRINO DETECTOR USING COMPUTATIONAL FLUID DYNAMICS

BY

DILLON PEDERSEN

A thesis submitted in partial fulfillment of the requirements for the

Master of Science

Major in Mechanical Engineering

South Dakota State University

2019

QUANTIFYING THE PERFORMANCE OF THE PROTODUNE SINGLE PHASE NEUTRINO DETECTOR USING COMPUTATIONAL FLUID DYNAMICS

DILLON PEDERSEN

This thesis is approved as a creditable and independent investigation by a candidate for the Master of Science in Mechanical Engineering degree and is acceptable for meeting the dissertation requirements for this degree. Acceptance of this does not imply that the conclusions reached by the candidate are necessarily the conclusions of the major department.

Stephen Gent, Ph.D.

Thesis Advisor Date

Kurt Bassett, Ph.D.

Head, Department of Mechanical Eng.

Date

Kinchel Doerner, Ph.D.

Dean, Graduate School Date

CONTENTS

LIST OF FIGURES

LIST OF TABLES

NOMENCLATURE

Acronym	**Meaning**
APA	Anode Plane Assembly
CPA	Cathode Plane Assembly
CERN	European Organization for Nuclear Research
CFD	Computational Fluid Dynamics
CISC	Cryogenic Instrumentation and Slow Controls
DUNE	Deep Underground Neutrino Experiment
Fermilab	Fermi National Accelerator Laboratory
GAr	Gaseous Argon
GHz	Gigahertz
LAr	Liquid Argon
LBNF	Long-Baseline Neutrino Facility
ppb	Parts Per Billion
S-Dr	Scalar Dissipation Rate
SST	Shear Stress Transport
T-ke	Turbulent kinetic energy
TPC	Time Projection Chamber

Term	**Meaning**
Boundary Condition	Physics specification at the limit of a region
Boussinesq Approximation	Buoyancy model based on a linear relationship between density and temperature

Buoyancy	Force acting on a body due to the displacement of a fluid
Cherenkov Radiation	Radiation emitted when particles travel faster than the speed of light through a medium
Cryogenics	Behavior of materials at very low temperatures
Cryostat	Region in the detector held at cryogenic temperatures
Dual-Phase Detector	New detector technology recording particle interactions in both liquid and gaseous argon for increased precision
Electron Lifetime	The average amount of time free electrons can exist in a medium before being absorbed
Field Cage	An enclosure used to block electromagnetic fields
Ground Plane	Plane used to ground the electronics in the TPC
Heat Flux	A flow of energy per unit area
Impurity	Any foreign body in a medium
Inertial Resistance	Resistance to a change in motion due to mass
Mesh	Discretized grid of two or three dimensional shapes used to numerically solve problems
Navier-Stokes Equations	Governing equations for momentum of a fluid
Natural Convection	Convection driven by differences in buoyancy
Neutrino	An electrically neutral subatomic particle with mass close to zero which rarely interacts with other particles
Nusselt Number	Ratio of conductive to convective heat transfer across a boundary

Passive Scalar	A scalar value that is effected by the flow, but does not affect the flow
Polyhedral Mesh	Mesh created by using cells with multiple sides
Porosity	Measure of empty space inside a medium
Prandtl Number	Ration of momentum diffusivity to thermal diffusivity
Residual Convergence	Occurs when residuals stay at consistent values over extended numbers of iterations
Schmidt Number	Ratio of momentum diffusivity to mass diffusivity
Shear	Strain produced when layers are shifted laterally
Single-Phase Detector	Detector technology using a single, liquid phase of argon to detect neutrino interactions
Slip, No-Slip	Shear specification indicating if there is fluid motion relative to a boundary
Surface Flux	A mass flux per unit area coming off of a surface
Tetrahedral Mesh	Mesh created by using cells with six equal sized sides
Time Projection Chamber	Region inside the detector where neutrino interactions are detected
Turbulence	Denoting fluid flow where velocity at any point fluctuates irregularly
Ullage	The amount by which a container falls short of being full
Viscosity	A quantity expressing the magnitude of internal friction
Viscous Resistance	Resistance to fluid motion due to internal friction

Symbol	Meaning
c_p	Specific Heat Capacity, or Pressure Drop Coefficient
k-epsilon	A common two equation turbulence model
k-omega	A common two equation turbulence model
ms	millisecond
ρ	Density
$\frac{D(x)}{Dt}$	Material Derivative
$\frac{\partial}{\partial t}$	Partial Derivative
∇	Covariant Derivative
$\vec{V}$	Velocity Vector
P	Pressure
μ	Absolute or Dynamic Viscosity
$\vec{g}$	Gravity Vector
$\vec{f}$	Force Vector
u	Velocity in the x-direction
v	Velocity in the y-direction
w	Velocity in the z-direction
τ_{ij}	*j*th component of the stress acting on faces normal to axis *i*
k	Turbulent Kinetic Energy
ω	Specific Rate of Dissipation
β	Thermal Expansion Coefficient
h	Enthalpy

$\dot{q}$	Energy Generation
div	Divergence Operator
ν	Kinematic Viscosity
c	Mass Scalar
R	Passive Scalar Source Term or Universal Gas Constant

ABSTRACT

QUANTIFYING THE PERFORMANCE OF THE PROTODUNE SINGLE PHASE NEUTRINO DETECTOR USING COMPUTATIONAL FLUID DYNAMICS

DILLON PEDERSEN

2019

The goal of this research is to provide scientifically-valid computationally generated data of the flow, thermal, and impurity data of the ProtoDUNE single phase detector. Results are compared and validated against an actual detector that is currently being utilized to collect temperature and impurity data. This research will investigate the flows inside these detection chambers using computational fluid dynamics to find approximate solutions to the governing equations of fluid mechanics. Impurity and flow data will allow researchers to determine if results collected are being obstructed by high levels of impurity. Novel approaches have been developed to strike a balance between accuracy and resource management as computation fluid dynamics software calculates information about the gaseous portion of the cryostat, which has limited amounts of data collection hardware. The Deep Underground Neutrino Experiment is a research collaborative attempting to investigate neutrinos. The ProtoDUNE single-phase detector is the second detector to be constructed by CERN for the DUNE project. The ProtoDUNE detector is being used to gather data and inform design decisions about the upcoming Far Detector, which is scheduled for completion in 2026.

1. INTRODUCTION

1.1 The DUNE Project

The Deep Underground Neutrino Experiment, or DUNE, is an experiment directed by the United States Department of Energy's Fermi National Accelerator Laboratory, or Fermilab. Fermilab is collaborating with the European Organization for Nuclear Research, also known as CERN, as well as over 1000 different researchers participating from over 175 different institutions located in over 30 different countries.

The DUNE project has several goals: explaining the origin of matter, finding a unified theory of forces and learning about black hole formation. The project is centered on learning how subatomic particles called neutrinos interact with matter. Researchers will be investigating differences in neutrinos and anti-neutrinos that could explain why matter exists in the universe. Finding evidence of proton decay will help in finding a unified theory of matter and energy. Neutrinos from supernova (exploding stars) would help with human understanding of black hole formation and could provide insight into neutron stars as well.

Neutrinos are subatomic particles that have a mass one millionth the size of an electron. There are three types of neutrino: electron, muon, and tau neutrinos. Neutrinos, like neutrons, have neutral electric charges. Neutrinos, due to their diminutive size and failure to interact with electromagnetic forces, do not interact with matter very often. The sun is constantly producing neutrinos, so much so that approximately 65 billion neutrinos per second pass through every square centimeter of Earth. They are also able to be

produced artificially in particle accelerators and from nuclear weapons and power plants. The DUNE project is looking at neutrinos produced from the sun, particle accelerators, and other cosmological events like supernova.

One is not able to detect neutrinos directly, instead, researchers must observe the interaction between neutrinos and matter. The most established procedure for observing this interaction is to have a neutrino collide with a larger particle and detect Cherenkov radiation. A neutrino interacting with a particle can emit photons or electrons. This release, known as Cherenkov radiation, can occur from any of the three types of neutrinos interacting with matter, however, it is currently impossible to determine which type of neutrino caused the Cherenkov radiation. To detect these emissions, highly sensitive photodetectors will detect any photons and large arrays of positively and negatively charged wires are set up to detect electrons.

From an engineering perspective, photodetectors must be designed in very precise ways to accurately measure neutrino interactions. To increase likelihood of an interaction, the detectors need to have a dense medium that is extremely pure and allows light and electrons to pass through it. The medium also needs to be inert. If the free electrons are absorbed, they cannot be detected. The conclusion is that an element from the noble gas column of the periodic table should be cooled to liquid state and purified to be used as the medium. Air is almost 1% argon, so it is very abundant, and is the medium of choice for the DUNE project. Argon has a boiling point of 87.3 K and the detectors need to be well insulated to stop heat entering the system and boiling the argon. Impurities, such as oxygen and water, will also absorb electrons before they can be detected, so the total impurity level of the detector must be less than 100 parts per trillion.

The amount of background light and electrical activity in ambient conditions on Earth's surface would interfere with the incredibly sensitive detectors. The detector needs to be far away from these sources of interference, so the Long-Baseline Neutrino Facility (LBNF) is being constructed a mile underground. The LBNF facility is being constructed at the Sanford Underground Research facility in Lead, SD. This facility is approximately 800 miles away from where some of the neutrinos will be produced, in Batavia, IL.

Due to the infrequency of neutrinos interacting with matter, the detectors will be built as large as possible to increase the likelihood of neutrino-matter interaction inside them. The LBNF will contain four separate detectors for a combined total of 68,000 metric tons of liquid argon. The configuration for the facility is shown in Figure 1.

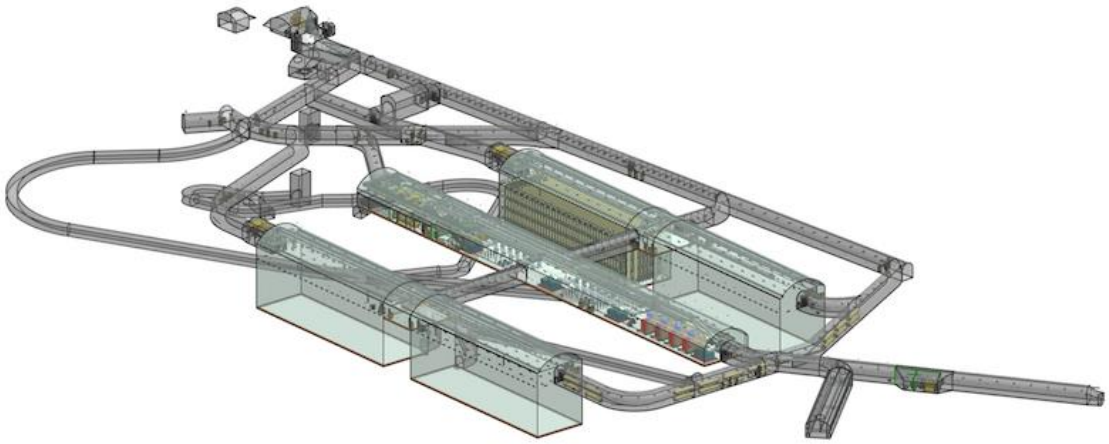

Figure 1.1 The LBNF facility designed to house four neutrino detectors (Fermi National Accelerator Laboratory, 2018)

The four largest chambers of the facility will each contain a 19 by 66 meter detector which is 18 meters tall. These detectors, in order to satisfy the requirements described to be able to detect neutrinos, have undergone an extensive design process by engineers and scientists from all over the world. This design process would not be complete without prototypes to test the components, software and systems necessary to keep the detectors online and free from contaminants. These prototypes are being

analyzed from a fluid dynamics perspective in order to create better designs for the LBNF detectors. The first prototype detector was the 35 Ton liquid argon detector tested at Fermilab in Batavia, IL. The second and third prototypes are the ProtoDUNE single-phase and dual-phase detectors. These detectors are being housed at CERN on the French-Swiss border. The ProtoDUNE single-phase detector is the subject of analysis for this thesis. These prototype detectors finished construction and began operation in Q3 of 2018.

The detectors are able to analyze interactions between the neutrinos and the medium inside the detector, which in the case of the DUNE project is liquid argon, by detecting photons and free electrons. When a neutrino hits an argon atom light and electrons will sometimes be released. If this happens in a specific region inside the detector known as the Time Projection Chamber, the electrons will be repelled by the Cathode Plane Assemblies and attracted to the Anode Plane Assemblies where the equipment can map in three dimensions where the interaction occurred. It is not only important that the detectors have very low contamination in order to increase electron lifetime, it is also important that there are no areas with high concentration of contaminants as it would make these areas less likely to show neutrino interactions when mapping. The graphic on the next page explains the major components and regions of the ProtoDUNE single-phase detector.

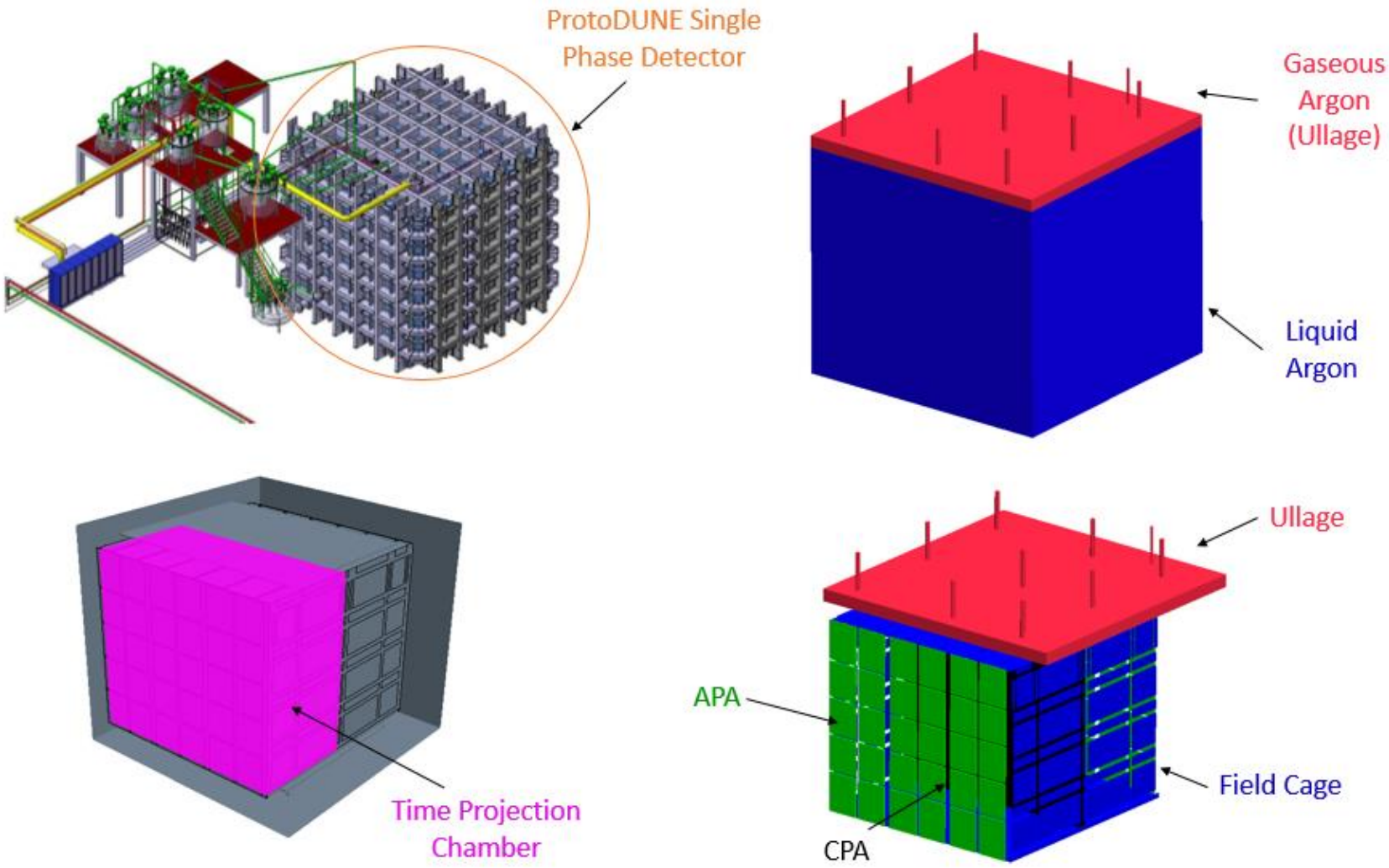

Figure 1.2 Important components and regions in the ProtoDUNE Single-Phase Detector

1.2 Modeling and Simulation

When modeling the fluid dynamics inside the cryostat, there are important aspects to consider that could change the quality of the solution of the CFD simulation. One of the major features of the model is that it is a flow almost entirely governed by natural convection. Other important aspects that need to be covered include modeling a cryogenic fluid and gas, correctly modeling the impurities in the simulation, making sure the simulation has enough refinement to ensure an accurate solution, and determining if the modeled boundary conditions are valid.

Due to the relatively small amount of liquid entering the system compared to the amount in the cryostat, almost all of the fluid motion is induced by small temperature differences. This is analogous to how hot air balloons float due to the air inside them being less dense than the cooler ambient air, so too will the argon move in the cryostat due to these temperature differences. The way the cryostat is designed is to let warmer liquid returning from the filtration system be reintroduced at the bottom of the cryostat. This warm liquid, being less dense, will then rise to the surface where small amounts of the argon boiling will take energy from the surrounding argon to vaporize, causing the liquid around it to get colder and sink. This is a modeling challenge because the temperatures need to be very precise to produce the correct flow profile.

As previously mentioned, because this is a natural convection driven flow, it is extremely important that the temperatures in the liquid and throughout the cryostat be correct. Modeling heat transfer correctly is another problem that needs to be looked at extensively to make sure the solution is accurate. This problem requires accurate

modeling of conductive heat transfer across the insulation whose conductivity changes depending on the temperature of the insulation. It also depends on correctly predicting the heat transfer coefficient from the insulation to the fluids. Finally, it requires correct heat transfer prediction between two fluids, the liquid argon and the gaseous argon.

Boundary conditions are used to define how a simulation interacts with everything outside of the simulation, and much of the complexity for the heat transfer comes from the boundary conditions. In reality, the detector will sit inside a large lab, which is in a building in Switzerland. The model only extends to the outer wall of the detector. There needs to be a condition saying that the temperature of the outer wall is the same temperature as the lab, or there is some amount of heat transfer occurring at the wall because of the air temperature of the lab. Likewise, there are boundary conditions in-between different regions in the cryostat that define how the regions can interact with each other. Interactions like “how much heat transfer will occur between the insulation and the fluid” or “is there a shear specification defining fluid motion relative to the wall”. These boundary conditions can be challenging to define as they are often simplifications. Boundary conditions may have a major impact on results so it becomes important to define them appropriately.

A majority of CFD work being done is for common fluids at normal working temperatures. CFD analysis on cars and planes is very common to learn about aerodynamics. It is also very common to use CFD when looking at air intakes and fuel pumps in engines or flow in a heat exchanger to find better designs and increase efficiency. Researchers know a lot about air and water at a wide range of temperatures because they are so commonly used in experiments and simulations. There are fewer

experiments or simulations done for less common fluids like liquid argon. This is a unique challenge because without a lot of published research on this fluid, it can be difficult to find extensive information on its properties.

Another important modeling consideration are the impurities in the liquid. Researchers hypothesize that the impurities are entering the liquid region from the ullage. Modeling the impurities could be as reductionist as assuming they are evenly spread throughout the cryostat or as intensive as tracking individual particles as they move through the argon. Ensuring an accurate solution is important to the operation of the cryostat, so assuming that the impurities would be evenly spread is an oversimplification that will not be of use to researchers. Tracking the particles individually would require excessive computational time and power. The ProtoDUNE project is on a schedule so simulations need to be run in a reasonable amount of time in order to provide design feedback while keeping the project on schedule. Instead, a compromise can be found between accuracy and computational expense. The amount of impurities in the liquid is in the range of parts per trillion, so one can neglect their effect on the flow. However, calculating how another species would diffuse throughout the flow would give useful information on the total amount and concentration of impurities at any location in the liquid. A passive scalar that calculates the diffusion of a species throughout a flow without effecting the flow fits both of these criteria.

Viscous fluid flows can be modeled by the Navier-Stokes equations. The mass and momentum equations are second order nonlinear partial differential equations. These equations can be, and have been solved for a select few simple cases such as flow between two infinite plates, i.e. Couette flow, and simple flow through a round pipe, i.e.

Hagen-Poiseuille flow. With every additional geometric configuration that effects the flow, the ability to analyze the flow analytically becomes increasingly more complex and impossible to solve analytically. So instead, the problem must be solved using numerical methods.

The final consideration for this problem is how to solve this problem with numeric methods that can give grid-independent solutions. A simple two-dimensional steady state conduction example in figure 1.3 shows how the size and refinement of a grid can affect the solution. This gets more complex in a fluid as more properties are included, such as motion, pressures, and turbulence. An unrefined grid could give a wrong solution in these cases.

	50	50	50	50	50	
30	37.81	39.54	38.86	36.07	29.06	10
30	31.69	31.52	29.81	26.36	20.17	10
30	27.43	25.02	22.50	19.40	15.27	10
30	23.00	18.64	15.77	13.48	11.49	10
30	15.94	10.76	8.45	7.28	7.19	10
	0	0	0	0	0	

	50	50	50	50	50	50	50	50	50	50	
30	39.36	42.67	43.88	44.22	44.08	43.57	42.59	40.82	37.36	29.73	10
30	34.77	37.45	38.64	38.90	38.53	37.60	35.98	33.32	28.91	21.54	10
30	32.27	33.73	34.32	34.22	33.55	32.32	30.41	27.57	23.41	17.54	10
30	30.59	30.86	30.69	30.11	29.13	27.71	25.76	23.13	19.64	15.19	10
30	29.24	28.41	27.47	26.39	25.14	23.63	21.81	19.56	16.81	13.57	10
30	27.96	26.08	24.39	22.86	21.38	19.88	18.27	16.48	14.48	12.29	10
30	26.53	23.55	21.16	19.25	17.66	16.25	14.91	13.60	12.33	11.13	10
30	24.61	20.43	17.44	15.33	13.76	12.53	11.52	10.69	10.11	9.88	10
30	21.50	16.10	12.86	10.85	9.53	8.60	7.93	7.54	7.55	8.27	10
30	15.27	9.60	7.04	5.70	4.91	4.40	4.08	3.98	4.29	5.64	10
	0	0	0	0	0	0	0	0	0	0	

Figure 1.3 Grid refinement effects on numeric two dimensional conduction

In order to be sure the solution is accurate, it must be grid independent, meaning the size of the cell does not affect the outcome of the simulation. A solution is grid independent if the same geometry and boundary conditions, discretized with different methods, can give the same solution.

1.3 Research Objectives

With the ProtoDUNE single-phase neutrino detector having started operation in late 2018, temperature and impurity data has been collected in great enough quantity to compare to simulation data. There are pumps that move liquid argon from the cryostat to the filtration system, then back after being filtered. Data has been collected for situations when these pumps are turned on and off.

The first goal of this research is to validate the simulation methods and boundary conditions used in the simulation by conducting a boundary condition sensitivity study and comparing temperature probe data from the physical detector to simulation data when the pumps are both on and off. Temperatures should be lower when the pumps are off because the liquid is returned to the cryostat at a higher temperature than when it is removed.

The second research goal is to use the impurity data collected from the physical detector to use as a reference to normalize the impurity data that was determined in the simulations. An unknown amount of contaminants is entering the liquid region during operation, so a simulation is performed using an arbitrary amount and that amount is scaled to what the impurity detectors found the true amount to be. With this data mapped, areas with high impurity concentration can be found and electron lifetime maps can be made.

The third research goal is to analyze the ullage. With far less data available in the ullage, simulations can be used to determine the amount of impurities being created in the gaseous portion of the cryostat, and different outgassing methods can be attempted to bring the total amount of impurities down. Using new techniques for sharing information between the liquid and gaseous simulations will be attempted to increase the accuracy of the simulated solution.

Gaining insight about the flow and impurity profiles of the single-phase detector is important to stopping potential problems with high concentrations of impurities ruining test results. Also, any additional information about how the detector operates, including changes to operating procedure, could help reduce impurities, increase the accuracy of neutrino experiments and help with the design of the LBNF detectors.

1.4 Organization of this Thesis

This thesis is organized in the following manner. Chapter 2 is the literature review, the state of the art in the modeling of the single-phase detector such as natural convection, computational fluid dynamics, fluid governing equations, and gas modeling. Chapter 3 is the methodology. Detail about the different geometries, boundary conditions, and processes that will be needed to attain accurate results for the simulations will be described in detail. Chapter 4 contains the results of the simulations alongside validation for the different boundary conditions and a discussion about usefulness of the information exchange occurring at the boundary between the liquid and the gas. Chapter 5 will have conclusions drawn from the thesis as well as some ideas for future work involving DUNE and the ProtoDUNE single phase detector.

2. LITERATURE REVIEW

This literature review section will provide detail and summarize computational fluid dynamics and the specific challenges that will need to be overcome to create an accurate model of the ProtoDUNE single phase detector. First, a historic perspective of CFD modeling and its transition from highly technical, hand-written pieces of code to its current state with many commercially available packages will be discussed to understand the background for these simulations. Next, the governing equations will be covered to examine how these commercially available packages solve a simulation. Then, a discussion will be held about the specific challenges outlined in the introduction and how other researchers have handled these situations. This discussion will include topics such as natural convection, cryogenic fluid modeling, modeling impurities, heat transfer, boundary conditions, cavitation, and discretization and grid independent solutions.

2.1 A Brief History of Computational Fluid Dynamics

In a 2003 newsletter, B.G.S. Prasad had commented on the state of the art of computational fluid dynamics in 1988. He had stated that “Nobody believed the result of a CFD calculation except the one who has generated it.” He would go on to say “Perhaps today an appropriate statement would be that most of the people believe the result except the originator” (Prasad, 2003). The process the development of CFD was long and laborious. Often times, simulations with as few as 11,000 cells would take days to create and even longer to run. 3D models could not be imported into software and visualization was less intuitive and less powerful. Three dimensional visualization would not exist until the turn of the century, and only simplified models could be run in any realistic amount of time. Even early on, with all of these problems, computational fluid dynamics

was able to deliver cost savings through improving designs (Brown, 2008). Gary Brown had been looking at an early simulation, first completed in 1995. In his paper, Brown stated “Using Moore’s Law as a guide, if computing power had doubled every 2 years for 12 years then the run time today should have reduced by a factor of 64 times, giving a run time of approximately 30 min. Incredibly, the simulation took only 1 min on a 2-GHz laptop.” CFD simulations have improved greatly, but they still do require validation and can quickly go wrong if improper modeling or physics are used. Verification can be tricky as well, as Fujii states “Unfortunately, the threshold has not been established in many flow physics, and the decision depends on a researcher’s experience” (Fujii, 2005). Over the years, commercially available code has been getting more popular. These software packages are easier to use and often come with theory guides that are a great reference for the theory behind fluid mechanics, how different models interact with the code, and what the best practices are when creating and simulating a model. This makes researchers less reliant on their own experience by giving them a large data bank to help make key modeling decisions. The top five most popular CFD software packages by total revenue are shown in the table below.

Table 2.1 Most used commercial CFD solvers from 1984 to 2014 (Hanna, 2015)

Position	**1984**	**1994**	**2004**	**2014**
#1	Phoenics	FLUENT	FLUENT	ANSYS (Fluent, CFX)
#2	FDIAP	FDIAP	Star-CD	Star-CCM+
#3	Fluent	STAR-CD	CFX	FlowTHERM
#4	Flow-3D	Flow-3D	FlowTHERM	PowerFLOW
#5	Scryu	FlowTHERM	PowerFLOW	Solidworks
CFD Market Size ($ million)	~10	~100	~430	~1,155
CFD Industry Average Growth Rate	~50%	~20%	~15%	~10%

This table ranks CFD software based on the total revenue. However it is important to note that there are open source and budget software packages, such as OpenFOAM, that are used every day and unaccounted for based on bringing in little or no money. It is no doubt that the two major commercial CFD packages are ANSYS' Fluent and recent Siemens' acquisition, Star-CCM+. These two packages are general packages. They are very good at most aspects of the modeling and simulation process. There are other CFD packages that are designed with more specific mindsets. FloTHERM is a CFD package designed specifically with pluming and heat transfer applications in mind. XFlowCFD is a package that solves models without first creating a mesh, instead using a Lagrangian approach to solve problems. Star-CCM+ was chosen to simulate the ProtoDUNE single phase detector due to previous experience with the software as well as the extensive theory guide provided to help with the modeling process. Figure 2.1 below are results from a survey for which programs CFD are most popular based on preference.

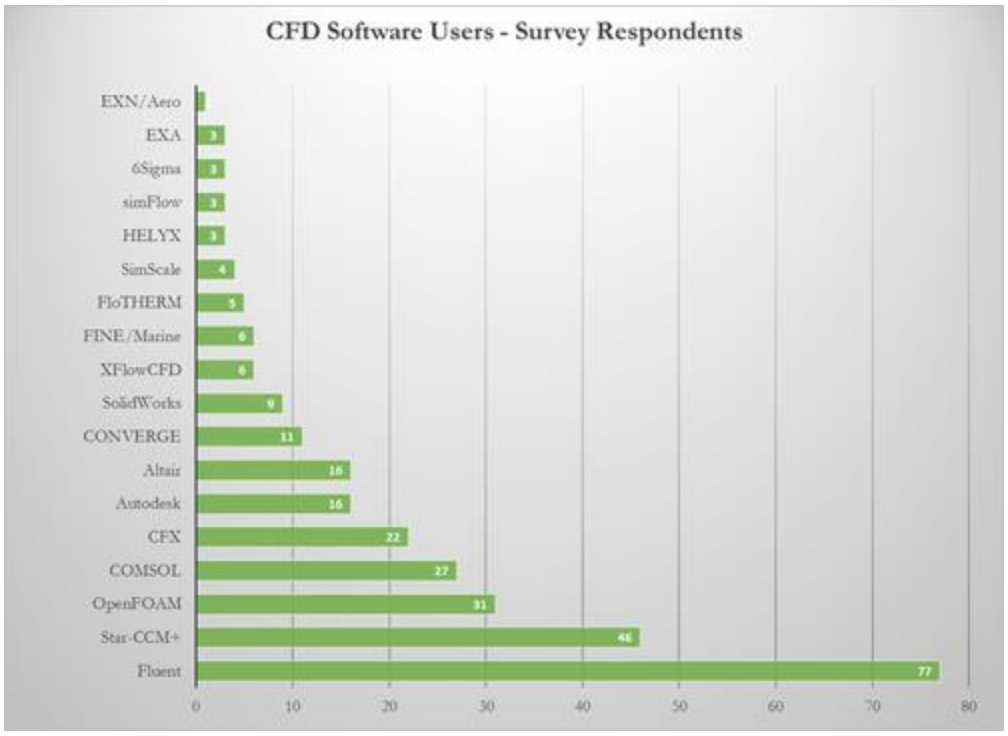

Figure 2.1 Informal poll results for preferred CFD package (Resolved Analytics, 2018)

2.2 Governing Equations

CFD packages attempt to find a solution to models by approximating numerical solutions to the fluid mechanics governing equations. Viscous fluid flow problems, like the one presented with the ProtoDUNE single phase detector, can be numerically solved by solving the Continuity Equation, the Navier-Stokes Equations (also known as the momentum equations), the Energy Equation, and because impurities are a key concern, Convection-Diffusion Equation.

2.2.1 The Continuity Equation

The continuity equation is an equation that underlies other transport equations such as the Navier-Stokes equation. When applied to mass, momentum, or energy the equation shows that the quantity in question must be conserved. When applied to a fluid

dynamics problem, it requires that mass entering the system must be equal to the amount of mass leaving the system and mass being stored inside the system. Equation 2.1 is the differential form of the continuity equation. Refer to the nomenclature section for definitions of variables.

$$\frac{D\rho}{Dt} + \rho\nabla\vec{V} = 0 \qquad \textbf{Eq. 2.1}$$

2.2.2 Navier-Stokes Equations

The Navier-Stokes equations are responsible for the conservation of momentum. These second-order non-linear differential equations describe the fluid motion of any viscous flow. The short hand form of the Navier-Stokes equations is shown in Equation 2.2.

$$\rho\frac{D\vec{V}}{Dt} = -\overrightarrow{\nabla}P + \mu\nabla^2\vec{V} + \rho\vec{g} \qquad \textbf{Eq. 2.2}$$

This equation can be expanded into three dimensions for problems being solved in the Cartesian coordinate plane which gives Equations 2.3, 2.4, and 2.5

$$\rho\left(\frac{\partial \mathrm{u}}{\partial \mathrm{t}} + u\frac{\partial \mathrm{u}}{\partial \mathrm{x}} + v\frac{\partial \mathrm{u}}{\partial \mathrm{y}} + w\frac{\partial \mathrm{u}}{\partial \mathrm{z}}\right) = -\frac{\partial \rho}{\partial \mathrm{x}} + \mu\left(\frac{\partial^2 \mathrm{u}}{\partial \mathrm{x}^2} + \frac{\partial^2 \mathrm{u}}{\partial \mathrm{y}^2} + \frac{\partial^2 \mathrm{u}}{\partial \mathrm{z}^2}\right) + \rho g_x \qquad \textbf{Eq. 2.3}$$

$$\rho\left(\frac{\partial \mathrm{v}}{\partial \mathrm{t}} + u\frac{\partial \mathrm{v}}{\partial \mathrm{x}} + v\frac{\partial \mathrm{v}}{\partial \mathrm{y}} + w\frac{\partial \mathrm{v}}{\partial \mathrm{z}}\right) = -\frac{\partial \rho}{\partial \mathrm{y}} + \mu\left(\frac{\partial^2 \mathrm{v}}{\partial \mathrm{x}^2} + \frac{\partial^2 \mathrm{v}}{\partial \mathrm{y}^2} + \frac{\partial^2 \mathrm{v}}{\partial \mathrm{z}^2}\right) + \rho g_y \qquad \textbf{Eq. 2.4}$$

$$\rho\left(\frac{\partial \mathrm{w}}{\partial \mathrm{t}} + u\frac{\partial \mathrm{w}}{\partial \mathrm{x}} + v\frac{\partial \mathrm{w}}{\partial \mathrm{y}} + w\frac{\partial \mathrm{w}}{\partial \mathrm{z}}\right) = -\frac{\partial \rho}{\partial \mathrm{z}} + \mu\left(\frac{\partial^2 \mathrm{w}}{\partial \mathrm{x}^2} + \frac{\partial^2 \mathrm{w}}{\partial \mathrm{y}^2} + \frac{\partial^2 \mathrm{w}}{\partial \mathrm{z}^2}\right) + \rho g_z \qquad \textbf{Eq. 2.5}$$

These equations would be able to capture turbulent effects if there was a grid small enough. A simulation this large would not be able to run in a reasonable amount of time if it had a grid small enough to capture these effects. The simulation will be run as a large eddy simulation, and use a turbulence model to account for the effects that cannot

be captured. The simulation will be solved as a large eddy simulation and to account for energy from eddy viscosity will solve the Reynolds-averaged Navier-Stokes equations and use the k-omega turbulence model shown in Equation 2.6a and 2.6b.

$$\frac{\partial(\rho k)}{\partial t}+\frac{\partial(\rho u_j k)}{\partial x_j}= \rho\tau_{ij}\frac{\partial u_i}{\partial x_j}-\beta^*\rho\omega k+\frac{\partial}{\partial x_j}\left[\left(\mu+\sigma_k\frac{\rho k}{\omega}\right)\frac{\partial k}{\partial x_j}\right] \quad \textbf{Eq. 2.6a}$$

$$\frac{\partial(\rho\omega)}{\partial t}+\frac{\partial(\rho u_j\omega)}{\partial x_j}= \frac{\gamma\omega}{k}\tau_{ij}\frac{\partial u_i}{\partial x_j}-\beta\rho\omega^2+\frac{\partial}{\partial x_j}\left[\left(\mu+\sigma_\omega\frac{\rho k}{\omega}\right)\frac{\partial\omega}{\partial x_j}\right]+\frac{\rho\sigma_d}{\omega}\frac{\partial k}{\partial x_j}\frac{\partial\omega}{\partial x_j} \quad \textbf{Eq. 2.6b}$$

2.2.3 The Energy Equation

The energy equation is responsible for the conservation of energy. This is equation accounts for the net rate of energy into a fluid element by means of a heat flux and the rate of work done due to body and surface forces. The differential form of this equation can be found in Equation 2.7

$$\rho\frac{Dh}{Dt}= \rho\dot{q}+div\left(k\vec{\nabla}T\right)+\tau_{ij}\frac{\partial u_i}{\partial x_j}+\rho\vec{g}\cdot\vec{V} \quad \textbf{Eq. 2.7}$$

2.2.4 The Convection-Diffusion Equation

The convection diffusion equation describes the physical phenomena of particles diffusing throughout a medium. This equation is necessary to be solved as the impurities in the liquid and gaseous regions will enter through specific surfaces and diffuse throughout the entire regions. Equation 2.8 describes how diffusion and convection transport the impurities throughout the system. The impurities will be passive and not affect the flow while being transported by the flow.

$$\frac{\partial \mathrm{c}}{\partial \mathrm{t}}=\nabla\cdot(D\nabla c)-\nabla\cdot(vc)+R \quad \textbf{Eq. 2.8}$$

2.3 Natural Convection

In his 2017 thesis, Propst outlined the creation of and best modeling practices for liquid systems driven by natural convection. Significant time was spent working on mixed convection, determining the best turbulence models to use as well as researching previous natural convection studies to inform modeling choices. The reader is encouraged to review (Propst, 2017) for full context. This research was highly valued as similar design choices were made in the liquid region of the ProtoDUNE detector. Additional information was required for this particular study. Specifically, the argon gas in the ullage would behave very differently that the liquid argon, and new methods would be needed to properly model this area.

2.3.1 Turbulence Modeling

In their paper, Zhang Zhai, Zhang, and Chen analyzed different turbulence models and their accuracy with respect to the computational time. This was done for natural convection cases, forced convection cases, mixed convection cases, and for strong buoyancy flow cases. The compared turbulence models included K-omega, K-epsilon, the modified v2f model, the detached eddy simulation, and others. The best models for natural convection cases were the K-omega model and the modified v2f model. The k-omega model was selected because the two models had similar accuracy but the k-omega model was able to be calculated in much less time.

2.3.2 Buoyancy Modeling

A method of determining the buoyant forces acting on the fluids is necessary to determining the flow profiles because the temperature will not be homogenous in the

liquid or gaseous regions. These methods will differ between liquid and gas due to the different temperature ranges that these fluids will experience.

2.3.2.1 Liquid Buoyancy Modeling

The density data needed to model buoyancy is limited to one data point because the temperature of the liquid is confined to such a limited range of approximately one tenth of a degree Celsius. The Boussinesq approximation can be used instead of a density model because of the very small range of temperatures found in the cryostat. Equation 2.9 describes the Boussinesq approximation.

$$(\rho_\infty - \rho) = \rho\beta(T - T_\infty) \qquad \textbf{2.9}$$

The Boussinesq approximation can be used in a liquid where the temperature range is very small, yet where buoyancy is still driving fluid flow. Gray and Giorgini say it can be used when the maximum temperature difference is less than or equal to 1.25 K. The temperature fluctuations that will be examined in the ProtoDUNE simulation are less than 0.1 K.

2.3.2.2 Gas Buoyancy Modeling

Initial tests of the gaseous region of the detector found that the temperature difference in the ullage could be upwards of 200 K under certain operating conditions. For a gas, the maximum temperature difference that can still be assumed accurate when using the Boussinesq approximation is about 28 K, therefore, the Boussinesq approximation is not valid for the gaseous ullage region.

The ideal gas law could be used as the buoyant model for this area. The ideal gas law is most accurate when modeling gases that are at low pressure and high temperatures. The ideal gas law is shown in Equation 2.10.

$$\rho = \frac{P}{RT} \qquad \textbf{Eq. 2.10}$$

When the pressure is held constant, the ideal gas law creates a linear density profile. The argon gas entering the ullage will be around 88 K, and at temperatures that low, the density is not linear with temperature. The ideal gas law would provide less accurate results than a polynomial density equation derived from the properties of argon gas at low temperatures.

Figure 2.2, derived from data provided the National Bureau of Standards, the nonlinear shape of the density of gaseous argon gives a clear indication of why neither

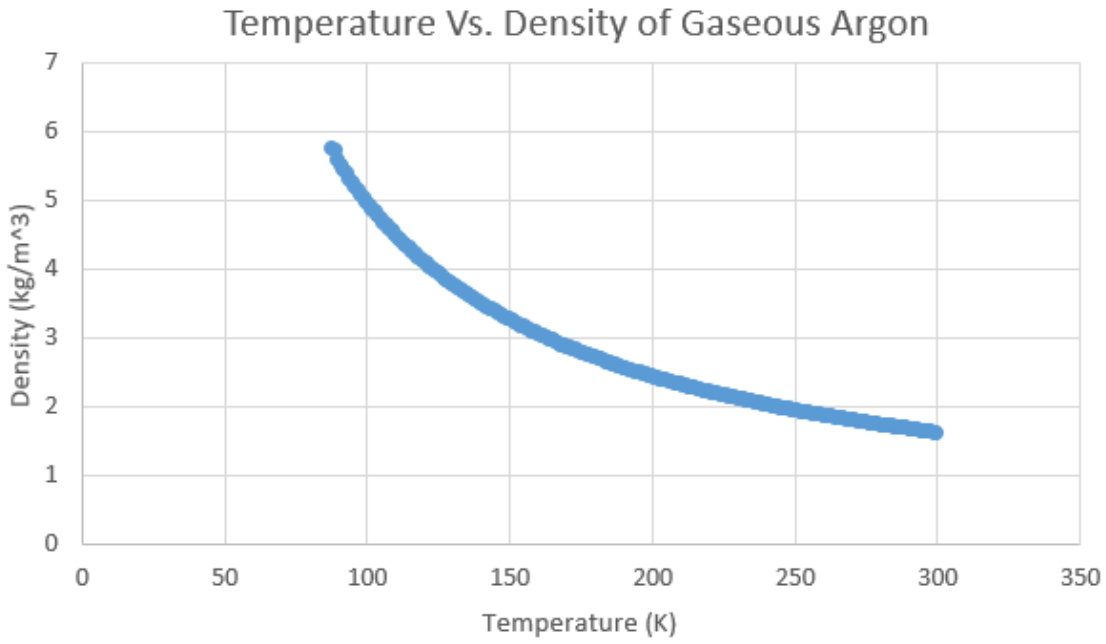

Figure 2.2 Density dependence on temperature for gaseous argon

the Boussinesq approximation nor the ideal gas law could properly describe the variable density phenomena of the ullage.

Equation 2.11 is the polynomial equation found from the data to be able to represent the density of the argon gas in the ullage, where temperature is in Kelvin.

$$\rho = -5.762 * 10^{-7}(T^3) + 4.315 * 10^{-4}(T^2) - 0.1149(T) + 12.737 \qquad \textbf{Eq. 2.11}$$

2.4 Heat Transfer

A study was done looking at how conduction through walls affected the natural convection of a two dimensional system. Misra and Sarkar looked at a square enclosure with a conducting vertical wall. They looked at the effect on the flow profile based on changing Rayleigh number, wall conductivity, and wall thickness. The Rayleigh numbers studied in the paper were orders of magnitude below the numbers expected in the ProtoDUNE detector. They found that the lower the thermal conductivity a wall has, the more non-uniform the temperature at the fluid would be. They also showed that with a thicker wall there is a smaller effective temperature difference, the driving potential for the fluid flow is reduced and the resulting flow diminishes (Misra & Sarkar, 1997). These points are important to consider when looking at the boundary conditions at the walls of the cryostat. Fermilab had provided heat flux data through the walls; using a constant heat flux would not account for the non-uniformity in the wall temperature profile as well as it would if calculating for conduction through the wall.

2.5 Boiling

A boundary that needs to be looked at in high detail is the boundary between the liquid and gaseous argon. The cooling at the surface occurs due to the vaporization of argon. Therefore, boiling will affect the real detector and should be considered in the

modeling process of the simulation. A study was conducted simulating a pool of liquid nitrogen boiling. Liu, Olewski and Vechot studied liquid nitrogen boiling into room temperature air. However, the only heat transfer occurred due to conduction from the ground the fluid rested on. There were no effects at the surface due to air temperature. Different ground temperature were tested ranging from 80K to 300K. The heat transfer occurring at the bottom of the fluid created a layer of vapor that would bubble off. They found that their simulation under predicted heat transfer for nucleate boiling, a type that could possibly occur in the ProtoDUNE detector (Liu, Olewski, & Vechot, 2015). The results of their simulations need to be considered when looking at temperature profiles in the ProtoDUNE detector. The ground or walls could potentially get warm enough to cause boiling. The places that this boiling would most likely occur would be corners and edges, boiling in corners and edges would have less impact than boiling in more open space. Only five to seven grams of argon would boil off each second compared to the 1.67 kg entering the cryostat per second and the total moving mass of approximately 800 tons, making any gaseous argon insignificant in the cryostat, even when accounting for difference in density.

2.6 Cryogenics

Other CFD experiments have been performed on tanks meant for holding cryogenic liquids. These simulations are generally for cryogenic liquids like hydrogen, due to its use as a fuel, and nitrogen, due to its abundance. One such paper by Ho and Rahman studied hydrogen being stored in a tank using a constant heat flux boundary condition through an insulated tank wall. His paper analyzed the mixing of the fluid as it entered the tank as well as the benefit of using a 3-D model compared to an axisymmetric

model (Ho & Rahman, 2008). Another paper used modern CFD analysis to study the liquid hydrogen fuel storage for the Saturn rockets. Their paper focused on sloshing in the fuel tanks. The simulation data that had been found for the ullage agreed with test data, finding that temperature from both the liquid and the ullage are dependent on local convection and vortices in the fluids. They also found that significant stratification occurred in the ullage (Grayson, Lopez, Chandler, Hastings, & Tucker, 2006).

Research into thermal stratification for cryogenic tanks has been accomplished as well. Choi, Lee, and Kim looked at the development of thermal stratification in cryogenic tanks holding liquid nitrogen based off heat flux conditions and pressure in the tanks. They found that higher heat fluxes cause stratification to occur more quickly and radial stratification occurred significantly less when the tanks were less full (Choi, Lee, & Kim, 2017).

2.7 Impurities

Modeling impurities in the detector came down to a decision between using a passive scalar and an active scalar. A passive scalar would follow the profile determined by the physics and movement of the liquid and gaseous argon without affecting it. An active scalar would be affected by the movement of argon while also affecting the movement of argon. A. F. Kurbatskii looked at the difference in turbulent diffusion between active and passive scalars due to convection using a Boussinesq model for buoyancy in 2003. He found that “A passive scalar in a thermally stratified medium more effectively diffuses from the surface source” (Kurbatskii, 2004). He also found that using the Boussinesq approximation for buoyancy increased the propagation time of the passive scalar compared to using a variable density buoyancy model. This is an important point

to consider as residuals may appear to have converged, but will actually converge on a longer time scale. There would be no point to let the passive scalar residual converge if there was no confidence in the result. Two of the best predictors of an accurate solution to a passive scalar are accurate Prandtl and Schmidt numbers. These numbers are defined as the ratio of momentum diffusivity to thermal diffusivity and momentum diffusivity to mass diffusivity. These two values greatly influence the amount of turbulent mixing that occurs. Combest, Ramachandran and Dudukovic explore the effects of these numbers on passive scalar transport in CFD simulations in depth. They found that setting constant global Prandtl and Schmidt numbers increased uncertainty, whereas defining them as a power series could help increase accuracy (Combest, Ramachandran, & Dudukovic, 1996). This may have been important while working on combustion models, but due to very low temperature changes, global values for these numbers would give a near identical level of accuracy in ProtoDUNE.

2.8 Grid Discretization

A two dimensional evaluation of the influence of grid refinement and boundary conditions in turbulent flow and convective heat transfer was conducted by Omri and Galanis. This experiment compared simulation data of different grid refinements to laboratory test data. These tests were done specifically to find methods for achieving a grid independent solution. The first result that were found was that the walls with temperature boundary conditions were found to have a grid independent solution for all of the fluid grids tested and had excellent correlation with experimental data. They also found that those walls with the adiabatic condition did not agree with experimental data. Their last major finding was that the number of nodes was not the most important factor,

but the distribution of nodes, which needed to be concentrated in the boundary layers (Omri & Galanis, 2007).

Juretić and Gosman studied the shape of the nodes instead of the distribution when determining sources of grid dependent error. They looked at three shapes of cells, quadrilateral, polygonal, and triangular, and the error in the pressure drop coefficient at different levels of discretization. An example from their report shows how these different node shapes are discretized in a channel with a cavity in Figure 2.3

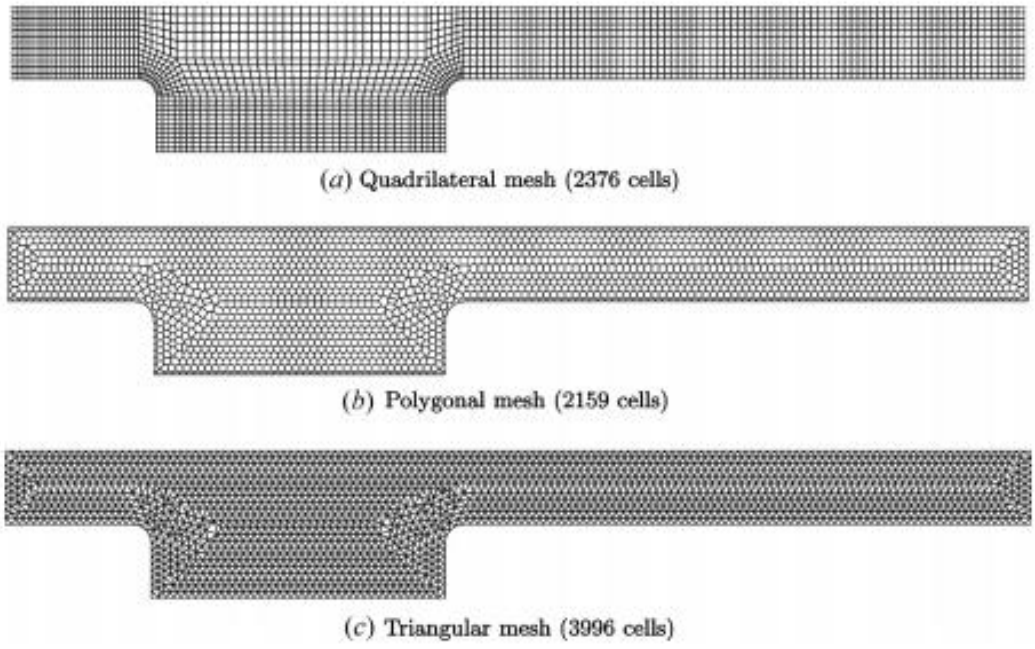

Figure 2.3 Different cell shapes in the same geometric configuration (Juretić & Gosman, 2010)

Table 2.2. from their paper shows that the quadrilateral and polygonal mesh types give similar amounts of error to each other, but produce much less error than the triangular cell type at similar cell counts.

Table 2.2 Pressure-drop coefficient at different cell counts for various cell shapes (Juretić & Gosman, 2010)

Pressure-drop coefficient (c_p)					
Quadrilateral		**Polygonal**		**Triangular**	
Cells	**c_p**	**Cells**	**c_p**	**Cells**	**c_p**
594	1.43128	556	1.59121	950	1.96345
2,376	1.49723	2,159	1.53935	3,996	1.67216
9,504	1.51544	8,487	1.52665	16,336	1.56432
38,016	1.51982	33,352	1.52333	65,430	1.53555
Mesh-independent value $c_p = 1.5203$					

2.9 Key Findings

- The k-omega turbulence model is the best type for large eddy simulations like those of ProtoDUNE.
- In the liquid region, the Boussinesq approximation should be used to model buoyancy.
- In the ullage region, a polynomial density model should be used to model buoyancy.
- Wall temperature may not be constant so conduction should be modeled instead of a constant heat flux on the walls of the fluid regions.
- Nucleation could occur anywhere, but it is most likely to occur near the edges and corners of the cryostat.

- Symmetric models of flow mixing in cryogenic tanks are less accurate than full models of flow mixing in cryogenic tanks.
- Cryogenic liquid and gas flows are highly dependent on local convection and vortices.
- Significant thermal stratification will occur in the ullage of a cryogenic gas.
- Using a Boussinesq model may take longer to iterate than using a variable density buoyancy.
- Distribution of cells is more important than total number. Boundary layers need higher concentrations of nodes than central areas.
- Quadrilateral and polygonal mesh types are more accurate at lower cell counts than Triangular

3. METHODOLOGY

In this chapter a thorough explanation of the geometry and methods used to simulate the Single Phase detector will be covered. The process for creating an accurate simulation of the cryostat started with the geometry for the liquid, gaseous, and solid portions of the cryostat. From there, different boundary conditions will be applied to simulate the proper amounts of heat transfer and fluid flow. Another important aspect of determining a reasonable representation were the physics models of the fluids being simulated. Proper physics models need to be included to fully capture the effects such as turbulence, heat transfer, density, viscosity, and thermal and inertial resistances etc.

The Time Projection Chamber (TPC) is a region inside the vessel that contains equipment for the detection of neutrinos. The TPC is most notably made up of the cathode plane assembly, two anode plane assemblies, a field cage, and an upper and lower ground plane. The TPC is inside the cryostat which is a large rectangular prism that will be sealed and filled with argon. The cryostat will be filled to 96% of the volume with liquid argon while the remaining 4% of the volume will be a gaseous argon ullage for the following several reasons. The ullage will exist at a lower pressure than the liquid because as the gas is pumped out causing liquid argon at the top of the cryostat to evaporate and cool down the liquid. This cooling of the liquid helps to remove the heat that will enter from the walls and because the liquid argon is returned slightly warmer than the liquid argon that is being pumped to the filtration system. The ullage is also designed to be a barrier for impurities entering the liquid portion of the cryostat. All of the argon that is being pumped out of the liquid region is sent to the filtration system to remove oxygen, water, and other contaminants before returning to the cryostat. The gas

pumped from the ullage is first condensed back to a liquid state before being recombined with the liquid argon and being pumped to the filtration system. In this analysis, the focus will be on the cryostat. An in-depth analysis of the filtration and cooling system for the argon is outside the scope of this thesis.

3.1 Model Assumptions

The CFD model was assumed to be operating at steady state. It was also assumed that the properties of the liquid argon remained constant. It was assumed that the temperature of the lab the vessel is in would be the temperature of the outside wall of the insulation. In areas where there was no insulation, such as the tops of the wire feedthroughs, a heat transfer coefficient of 5 W/m^2 was used in conjunction with the temperature of the lab to determine heat transfer. Researchers had expressed that due to temperature variations the cryostat could expand and shrink by a couple centimeters. The precise height of the liquid argon inside the cryostat could change. Geometric transience, however, was not taken into consideration when modeling the cryostat. This transience would not, in comparison to the scale of the simulation, have significant effects on the flow. Five to seven grams of argon is boiling off at the surface per second and providing cooling for the liquid. The simulation did not include the top surface as an exit for the argon. Rather, all liquid argon left through the outlet at an approximate rate of 1.668 kg/s.

3.2 ProtoDUNE Single Phase Liquid Region

3.2.1 Geometry

The geometry for the ProtoDUNE single phase detector is a large rectangular vessel filled with liquid argon. The vessel's base has inner dimensions of 8.548m by 8.548m, the distance from the floor to the ceiling inside the cryostat is 7.9m. Inside the cryostat there are several important features that are used in the detection of neutrinos. The detector itself is the main concern of the CFD simulation. Figure 3.1 shows the external geometry of the vessel while the internal geometry of the detector portion of the cryostat is shown in Figure 3.2.

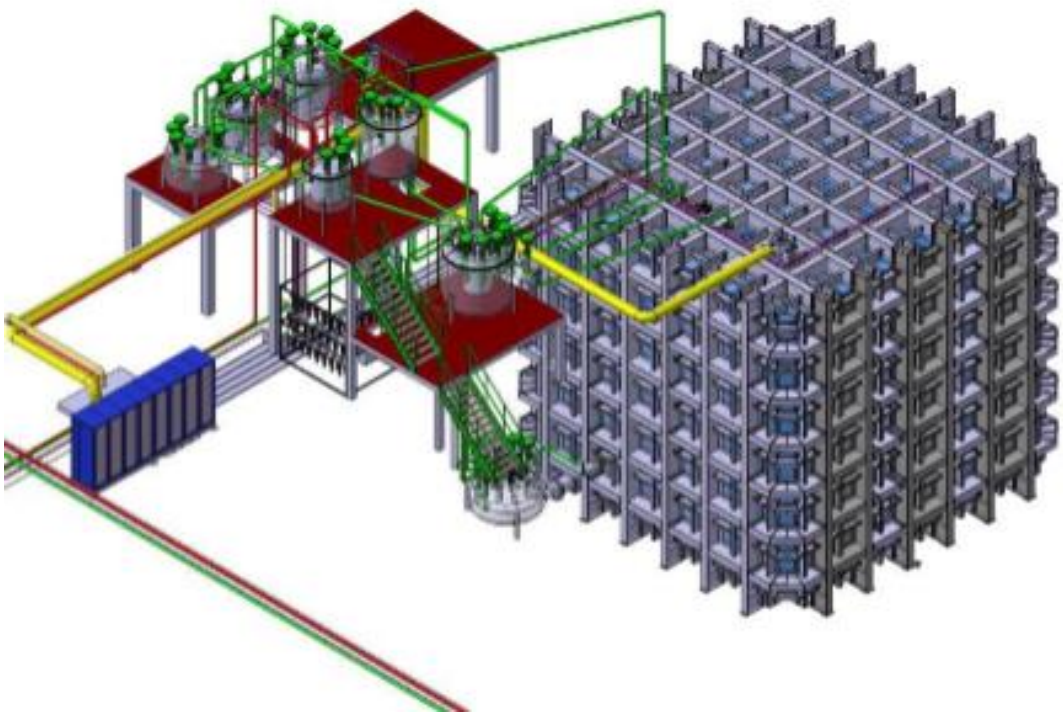

Figure 3.1 External geometry of the vessel and filtration system (Collaboration, Tdune, 2017)

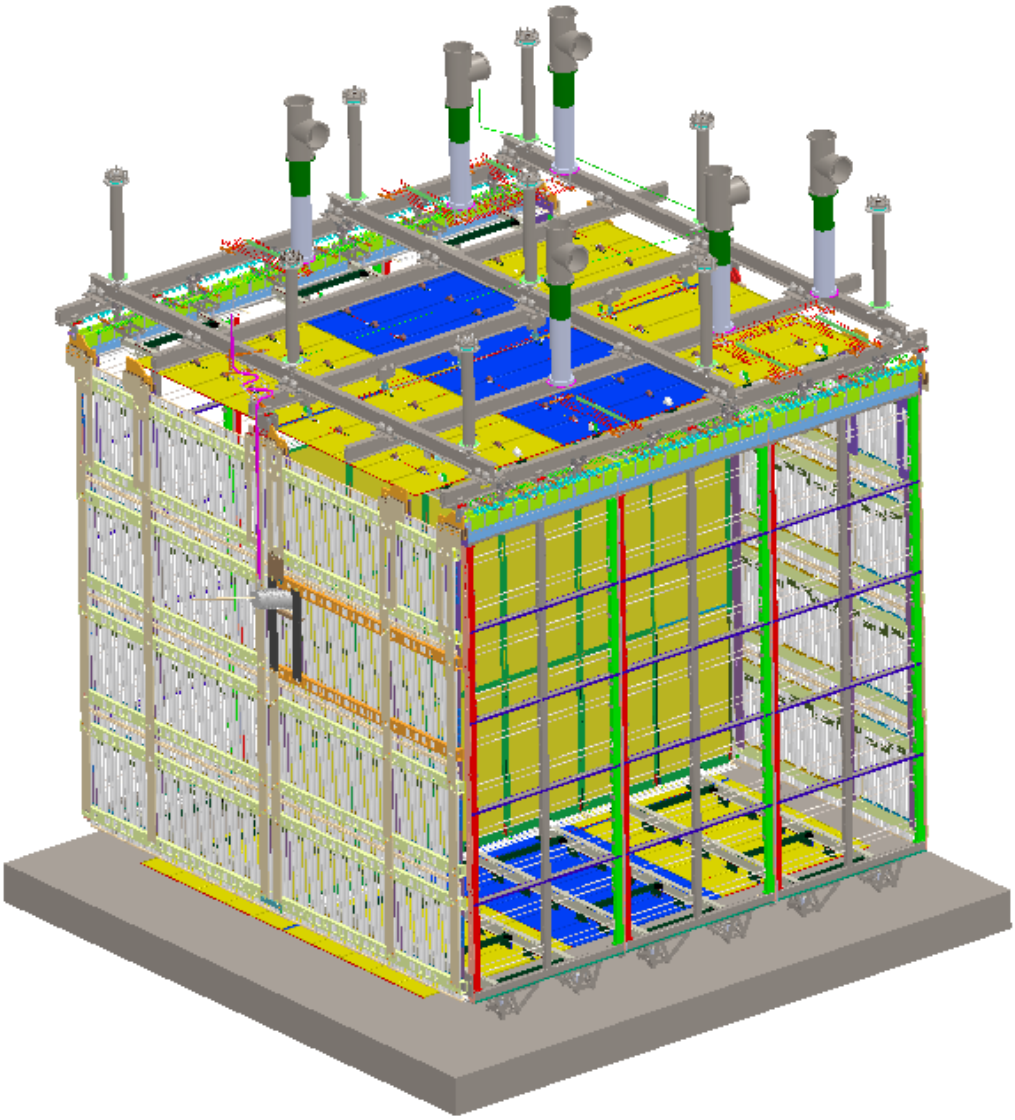

Figure 3.2 Full internal geometry

This complex geometry needed to be simplified to be able to both mesh and run the simulation in a reasonable amount of time. The amount of processing power available at South Dakota State means accurate simulations should be able to run in less than a week on the computing cluster. Increasing detail in models and running much longer than this will allow fewer resources to be available to other researchers and diminishing returns means these resources can be better used elsewhere. The most important features, the Field Cage, Anode Plane Assembly, Cathode Plane Assembly, and Ground Planes,

are shown in the figure below. The APA, Field Cage, and Ground Planes are all shown as solid objects in this geometry, however, as these are volumes with small and complex geometric features, such as wire arrays, they are imported as solid but are constrained as a porous region.

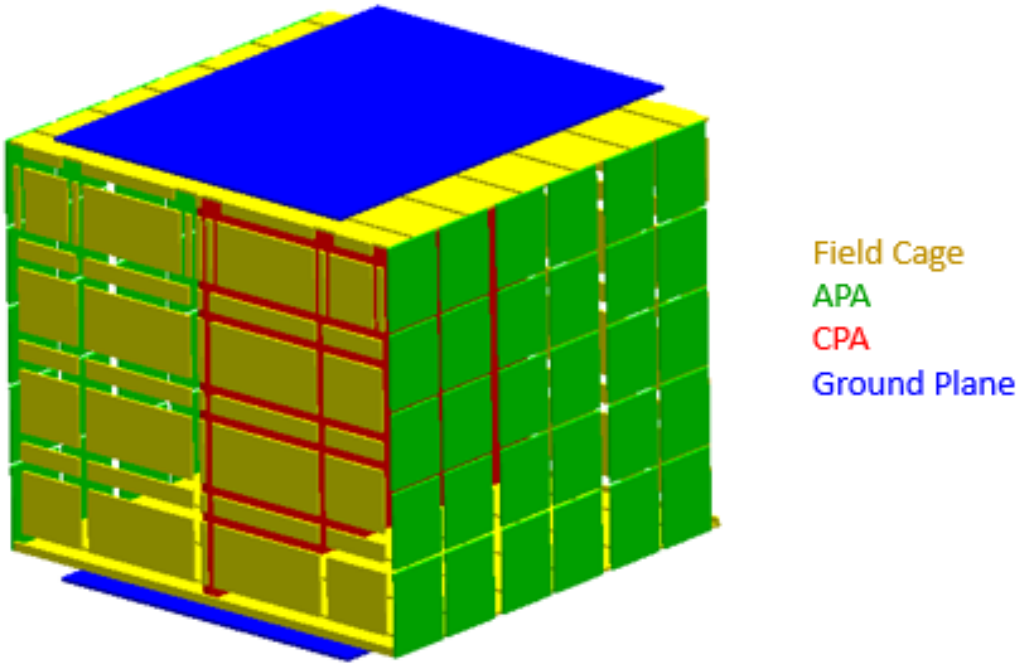

Figure 3.3 Simplified geometry

The locations of where liquid argon is pumped into the cryostat and where it is pumped out of the cryostat and into the filtration assembly, which is outside the scope of this research, are shown in Figure 3.4.

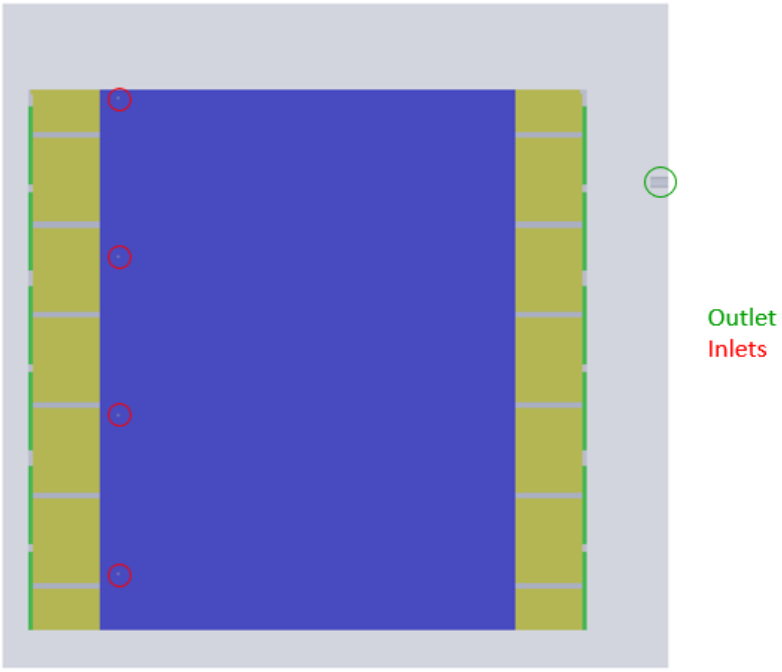

Figure 3.5 Bottom view of the cryostat showing locations of inlets and outlet

A cross section of the insulation that will help maintain the liquid argon temperature is shown below. It is a relatively complex geometry, but the main barrier to heat entering the system are the large insulation panels.

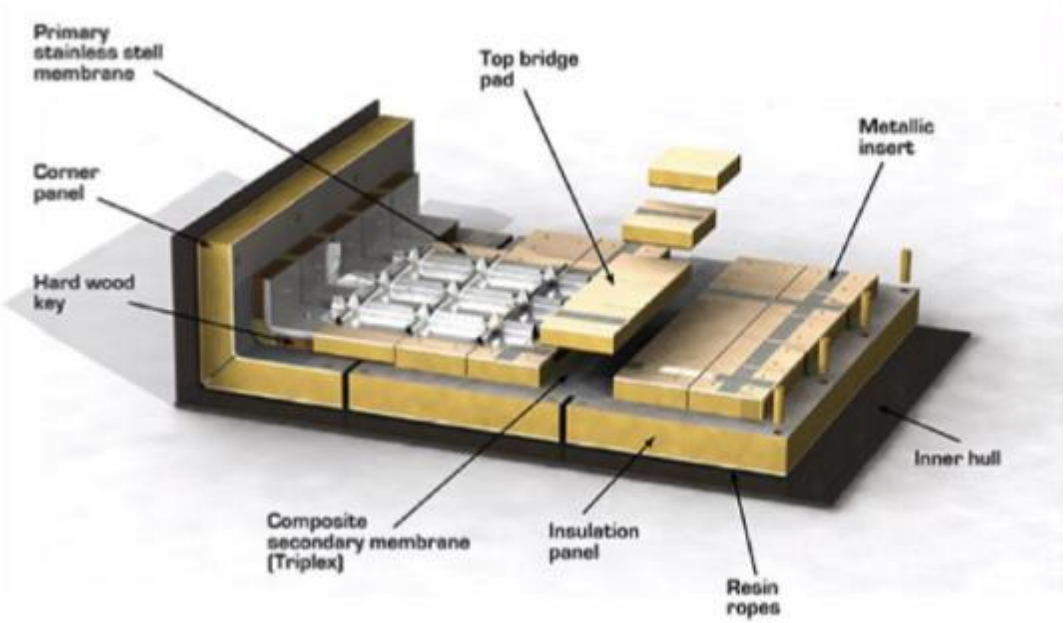

Figure 3.4 Insulation cross section (Collaboration, Tdune, 2017)

Again, as almost all of the thermal resistance is due to the insulation, only this part is modeled and less important pieces are ignored in order to save on the necessary computational resources being used for the simulation. A cross section of the insulation used for the simulation is shown below in Figure 3.6

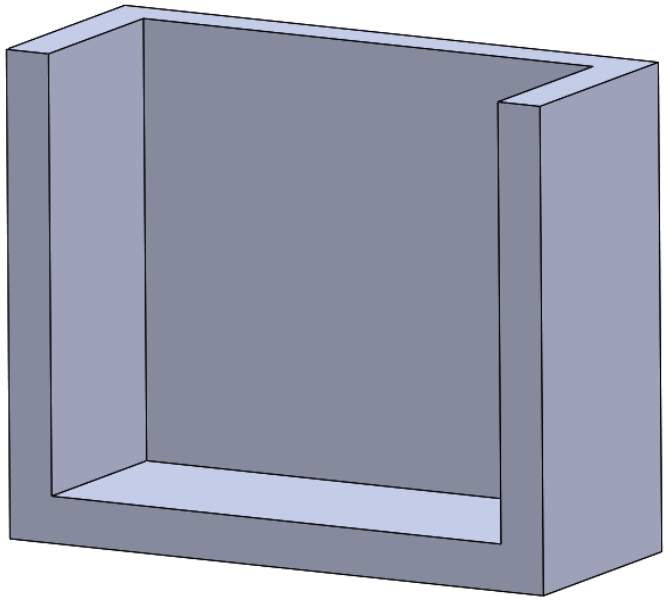

Figure 3.6 Simplified insulation cross section

3.2.2 Boundary Conditions

3.2.2.1 Heat Transfer between the Cryostat and Laboratory

Several different combinations of boundary conditions were tested to ensure accuracy in the results. The CISC researchers had estimated a value of 3 kW of heat flux entering through the insulated walls of ProtoDUNE. This value was used in early simulations and compared to a different condition which used the ambient temperature of the detector housing and calculated for conduction through the ProtoDUNE insulation. The temperature boundary, after simulations done at South Dakota State were analyzed, were found to be 2.7 kW. This more precise number comes from better conductivity data

provided by the manufacturer of the insulation. A temperature dependent equation is used in the simulations to determine conductivity. This equation is proprietary and is not included in this thesis.

3.2.2.2 Boundary Conditions at the Interface between Liquid and Gaseous Argon

Two different categories of boundary conditions were tested at the surface of the liquid argon. The first boundary condition is the shear specification. This boundary condition was tested with two options, slip and no-slip. The difference between these two is whether the liquid at the boundary is allowed to have any velocity relative to that boundary. Slip means that the liquid is allowed to have a velocity while no-slip means that the liquid is not. This boundary condition could have a large impact on the heat transfer that occurs at this surface.

The thermal specification at the surface was also tested with two different options, a constant surface temperature based on the temperature of the ullage, or a constant heat flux based off of the heat of vaporization of argon as well as the amount of argon being removed from the ullage through the gaseous argon purges.

It was unknown which combination of these boundary conditions most correctly modeled the heat transfer occurring at the surface of the liquid, and therefore, a scenario would need to be run for each combination of these boundary conditions.

3.2.2.3 Pumps Returning Liquid from the Filtration System going Offline

Another boundary condition consideration was the mass flow rate of the inlets. Under normal operating conditions the outlets will each have a flow rate of 0.4152 kg/s. The thermal profiles of the CFD model are compared with static and dynamic thermocouples in the ProtoDUNE detector to determine the validity of the boundary conditions and

physics models. If the simulation gives agreeable data for when the pumps are off as well as on, then it can be confirmed that the modeling approach is valid for additional studies of the ProtoDUNE detector.

3.2.2.4 Viscous and Inertial Resistances of Porous Regions

There are two regions with very small geometric patterning in relation to the size of the entire detector. These regions are also incredibly important to the flow profile developed by the model. The APA planes are large rectangular frames with an intricate mesh of wires that are used to detect ionization cause by the neutrinos interaction with the liquid argon. These wires may be modeled and meshed given enough time and computing resources, but the level of fidelity that would be needed would cause all but the most powerful computers to run out of internal memory long before the mesh could be generated. Even if it were to be run on a powerful enough computer, the amount of time it would take to simulate would be enough of a reason not to model this plane in this manner. Instead, previous research at Fermilab and at SDSU has provided a clear path forward to solving this problem. Rather than modeling the individual wires in the cryostat in their entirety, they can be modeled with the same footprint as a homogenous porous region. The porous region has both viscous and inertial resistance amounts that can be used to compute a pressure drop across the region. In his thesis, Propst examines a section of the APA and the ground planes in depth to determine the appropriate viscous and inertial resistances for these regions. A unit cell section of the plane small enough to accurately include the wire array was simulated and from it the pressure drop determined. Next the viscous and inertial resistance coefficients were found from a trend line using the velocity as the independent variable and the pressure drop as the dependent variable.

These values were checked using a porous region with the determined viscous and inertial resistances in place of the wire array. The pressure drop values found when using the porous region were identical to the values found when using the wire array so it was determined that modeling the wire arrays as a porous region would be an acceptable way to simplify the geometry. The values for the field cage were found in a similar way, but instead of using an array of wires, the geometry of the field cage is slotted.

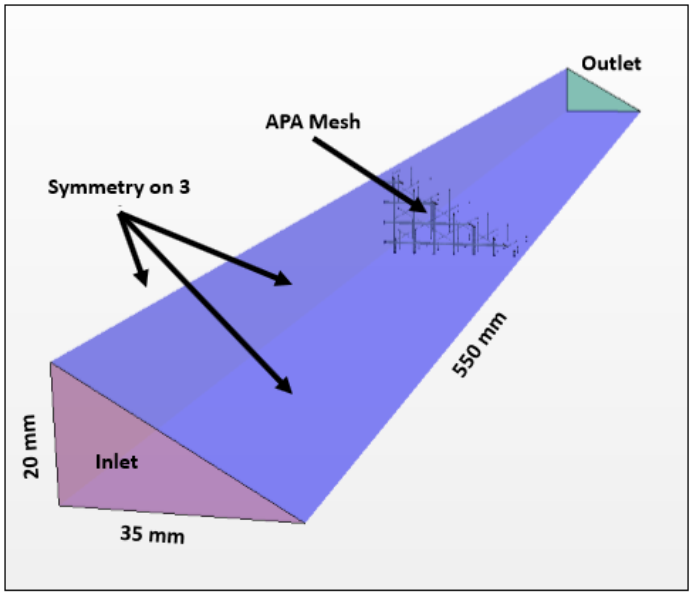

Figure 3.8 Pressure drop simulation for the APA (Propst, 2017)

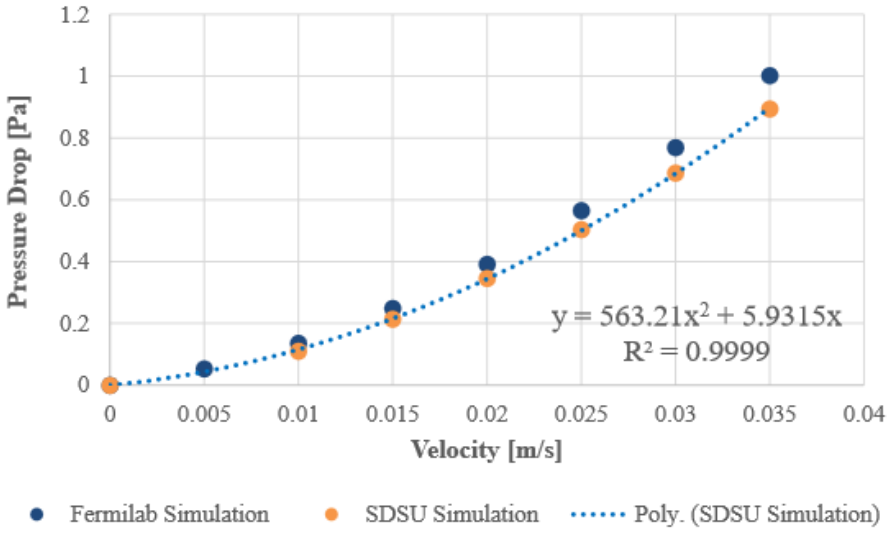

Figure 3.7 Plot of pressure drop vs. velocity, with coefficients used to determine resistance values. (Propst, 2017)

The variable and permanent boundary conditions for the liquid argon simulation are compiled in Table 3.1 below.

Table 3.1 Boundary conditions used for this study

Liquid-Gas Interface	Temperature: 87.593 K Heat Flux: 15.4 W/m^2 Shear Specification: Slip or No-Slip
Solid Walls	Temperature (insulated): 26.1 °C Heat Flux (non-insulated): 5.76 W/m^2
Inlets	Mass Flow Rate: 0.4152 kg/s (per inlet) or 0 kg/s Temperature: 88.1634 K
Field Cage	Porosity: 0.23 Viscous Resistance: 247.38 kg/m^3-s Inertial Resistance: 411280 kg/m^4
APA	Porosity: 0.73 Viscous Resistance: 118.63 kg/m^3-s Inertial Resistance: 11264.2 kg/m^4
Ground Plane	Porosity: 0.1 Viscous Resistance: 4007 kg/m^3-s Inertial Resistance: $2.37*10^7$ kg/m^4

3.2.3 Liquid Modeling

The fluid was modeled by segregating the mass, momentum, and energy equations when solving each iteration. The fluid was modeled as incompressible with constant properties. Because of this, the Boussinesq approximation was used to find the buoyant forces which drove the flow. The flow was assumed to be turbulent as the geometry of the cryostat would induce turbulence. The K-Omega turbulence model was used to predict the turbulence in the simulation. The density of the liquid argon was 1387 kg/m^3. The dynamic viscosity was $2.4982*10^{-4}$ Pa-s. The thermal conductivity was 0.12647 W/m-K

3.2.4 Validation

With the ProtoDUNE single-phase cryostat currently filled with argon and running, data can be collected about the temperature and impurity levels where those sensors exist. These sensor locations can also be added to the CFD simulations to look at how accurate the simulation is in comparison to the experimental values. Figure 3.9

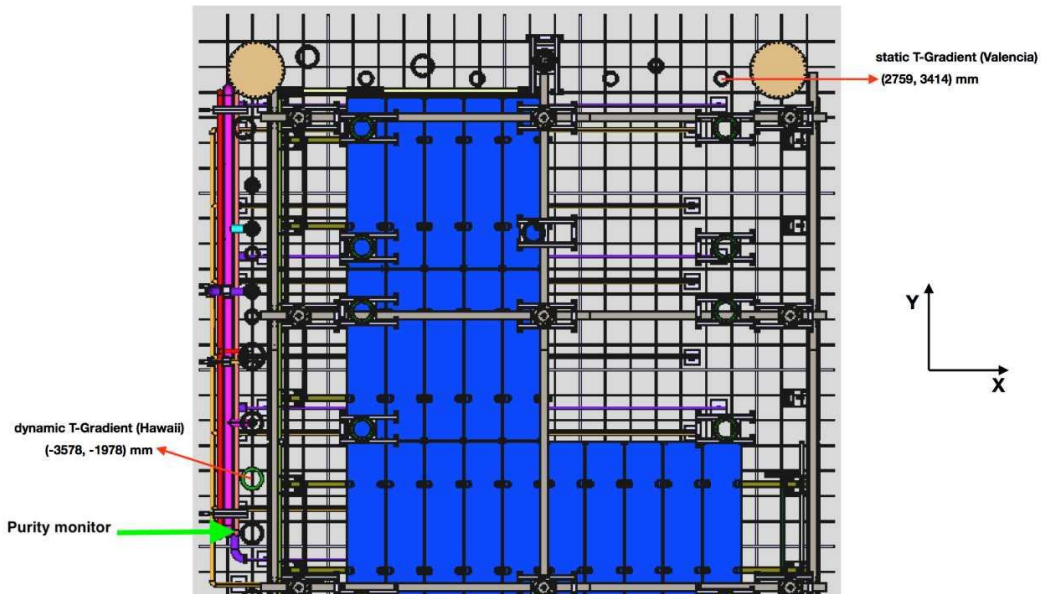

Figure 3.9 Sensor locations in the cryostat (Cervera & Seong, 2018)

shows the locations of the impurity sensor as well as the static temperature sensor array and the dynamic temperature sensor.

The three main sensors used in this research are a static temperature probe array with forty six sensors, a dynamic probe with three sensors that can be moved vertically and an impurity monitor with three sensors at various elevations.

3.3 ProtoDUNE Single Phase Ullage Space

3.3.1 Geometry

The full geometry outer geometry of the cryostat and insulation is shown below with feedthroughs entering through the top. These are suspension structures with conduits so that electrical signals ranging from temperature data to neutrino collection results can be analyzed in real time. The total capacity of the cryostat is approximately 580 m^3, however, in order to prevent contaminates from entering the liquid directly, about 4% of the cryostat is left as argon gas rather than filling it to 100% capacity with liquid argon. The idea behind this is that by pulling gas out of the cryostat, contaminants that enter through the top will be suctioned off before they can come into contact with the liquid surface. It also allows for cooling of the liquid argon at the surface due to the vaporizing argon from the slightly lower pressure in the ullage.

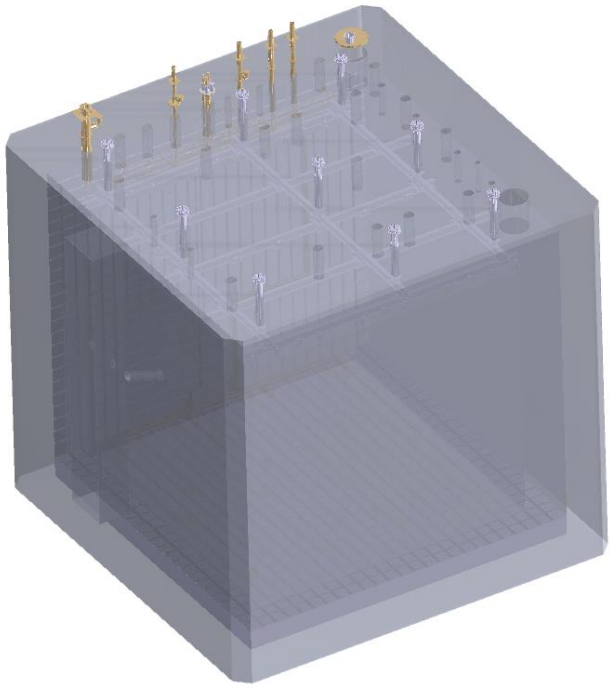

Figure 3.11 ProtoDUNE single phase exterior geometry

The Figure below is the top 4% of the entire cryostat. This is the portion of the entire cryostat that will be simulated as a gas instead of a liquid. There are many visible penetrations in the roof of the cryostat for instrumentation and structural support. Some of these will be closed off entirely after the detector is in operation.

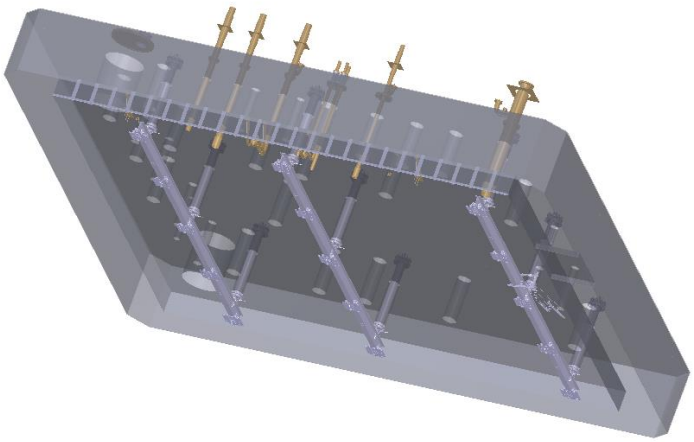

Figure 3.10 The top 4% of the cryostat volume is ullage space

Below is a simplified model of the region that will be simulated. It consists of nine feedthroughs. The model below is simplified with those penetrations thought to be most important. They are thought to be the most important because of the locations dispersed throughout the cryostat, the function, and the effect that they have on the purity of the gas. These feedthroughs are hollow cylinders. It is assumed that the inside of these cylinders are the warm surfaces that impurities are entering through. The tenth and smallest protrusion is the main outgassing channel for the ullage. While all feedthroughs have outgassing, currently, approximately 99% of the outgassing will occur through this main channel. These outgassing percentages are subject to change and alternative outgassing procedures will be tested with simulations.

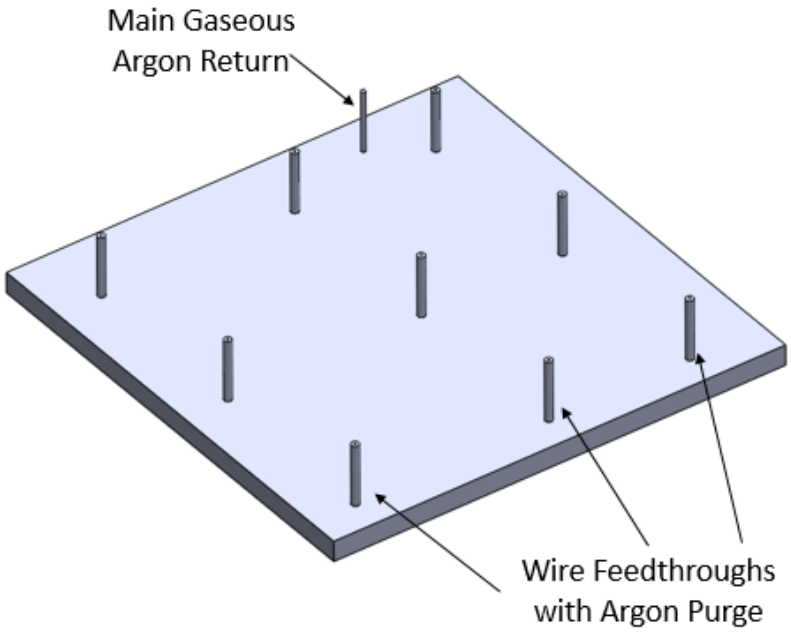

Figure 3.12 Simplified ullage volume

The Figure below shows the solid components of the ullage simulation, including the insulation and three I-Beams that suspend the detector in the liquid argon.

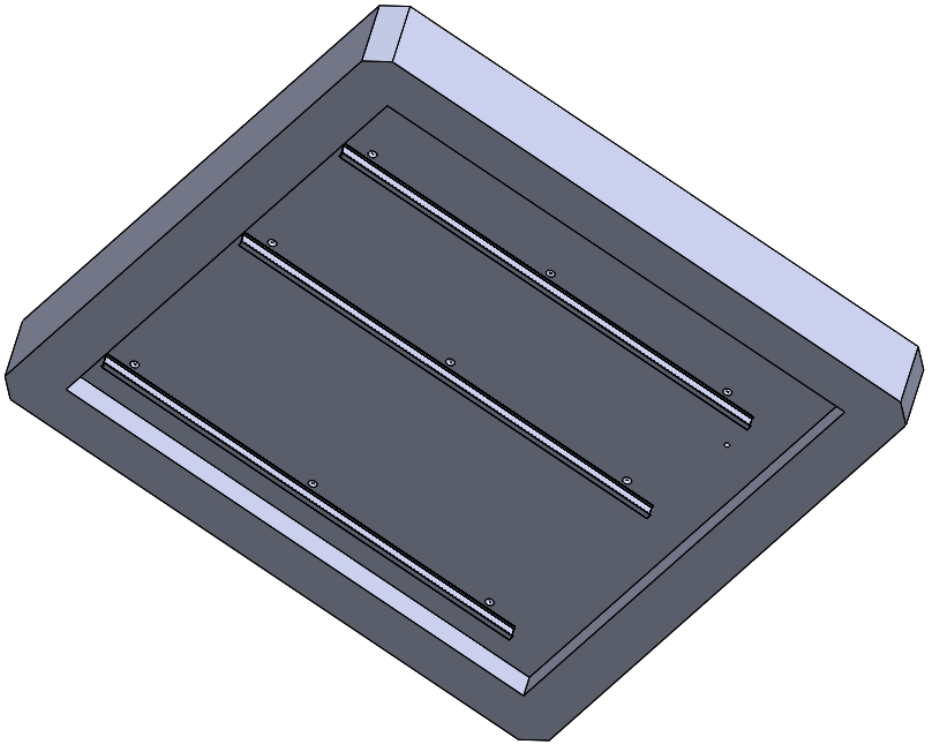

Figure 3.13 Ullage insulation and I-beams

3.3.2 Boundary Conditions

The boundary conditions for this model can be found in the table below

Table 3.2 Boundary conditions for ullage simulation

Inlet	Mass Flow Rate: 7.0 g/s Temperature: 88 K
Walls	Temperature: 26.1 °C
Gaseous Argon Outlet	Percent of Outflow: 99%
Chimney Purge Ports	Percent of Outflow: 1%

Table 3.3 Alternative boundary conditions for the ullage simulation

Inlet	Mass Flow Rate: 7.0 g/s Temperature: 88 K
Walls	Temperature: 26.1 °C
Gaseous Argon Outlet	Percent of Outflow: 1%
Chimney Purge Ports	Percent of Outflow: 99%

3.3.3 Gas Modeling

Several different gas models were used in order to account for the changes in buoyancy due to the temperature gradient present in the ullage. A Boussinesq approximation was used first but was ultimately removed due to the scale of the temperature gradient. Polynomial density, Peng-Robinson, Soave-Redlich-Kwong and Van der Waals models were each used to simulate the gaseous argon. The polynomial density physics condition was chosen to represent the gas because tabular information was available for the specific temperatures and pressures occurring in the simulation. Equation 3.1 was found using tabular data from the United States Department of Commerce National Bureau of Standards publication titled "Thermodynamic Properties of Argon from the Triple Point to 300 K at Pressures to 1000 Atmospheres" and is shown below (U.S. Department of Commerce National Bureau of Standards, 1969).

$$\rho = -5.762 * 10^{-7}(T^3) + 4.315 * 10^{-4}(T^2) - 0.1149(T) + 12.737 \qquad \textbf{Eq. 3.1}$$

3.4 Mesh Generation

In order to numerically solve the Navier-Stokes equations, the fluid volume contained within the cryostat must be discretized into a mesh of finite volumes. The trimmed cell mesher in Star-CCM+ discretizes the geometry into rectangular prisms where it is possible and polyhedrals near curved edges. In the literature review it was discussed that the two best options for grid discretization are the polygonal and quadrilateral mesh types. They are able to find a grid independent solution with fewer cells than the triangular type. An approximate solution needs to be calculated for each cell, so having fewer cells reduces the total amount of time is needed to find a solution. Testing done between the polygonal and quadrilateral mesh types at SDSU showed that the quadrilateral mesh type was discretized over ten times faster than the polygonal type.

Another way to save computational resources is to have a high level of grid refinement in regions that have intricate flow and thermal gradients such as solving fluid flows near boundaries, and less definition where the equations are much less complex, such as conduction through the solid insulation.

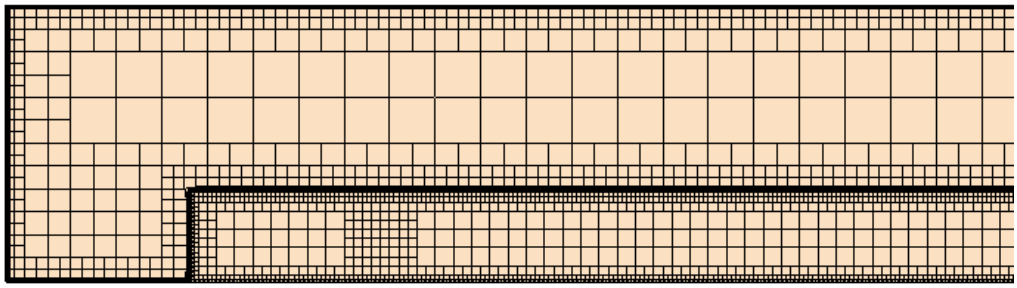

Figure 3.14 Mesh size decreases near areas that are harder to solve

Each simulation has multiple regions, however, ultimately there are two types of regions. The first type of region is the fluid region, this is where the liquid or gaseous flow is calculated. The second is the solid region. This region is primary used in

calculating the temperature of the insulation as well as solid portions that exist inside the cryostat. Figure 3.4 shows the amount of cells in each region type for both the liquid and ullage simulations.

Table 3.4 Cell counts in the liquid and ullage simulations

Simulation	**Fluid Cells**	**Solid Cells**	**Total Cells**
Liquid	6,300,00	9,000,000	15,300,000
Ullage	12,000,000	3,670,000	15,670,000

Number of cells may be correlated with proper discretization, however, there are other indicators that can determine if the simulation will arrive at a solution that is not dependent on the grid. A grid must be valid before a solution, grid independent or not, can be run. If a mesh has unclosed cells, invalid cells, zero area faces, or zero or negative volume cells the discretization is invalid and a simulation cannot be run. The STAR-CCM+ User Guide (Siemens, 2018) states that “In general, a poor quality volume mesh does not necessarily result in solver run time problems, but it does reduce the accuracy and efficiency of the solution obtained.” This means that more cell quality tests need to be done before running the simulation to see if further discretization is needed for a quality solution. According to the STAR-CCM+ User Guide, In regards to cells, cell faces should be normal to the cell centroid, have an even geometric distribution, have a volume equal to or larger than its neighbors, have a low skewness angle, not form a chevron with its neighbor, have its centroid be similar in distance from neighbor centroids, and not be warped. Figures below show some of the ways a cell can be considered poor for the sake of simulation.

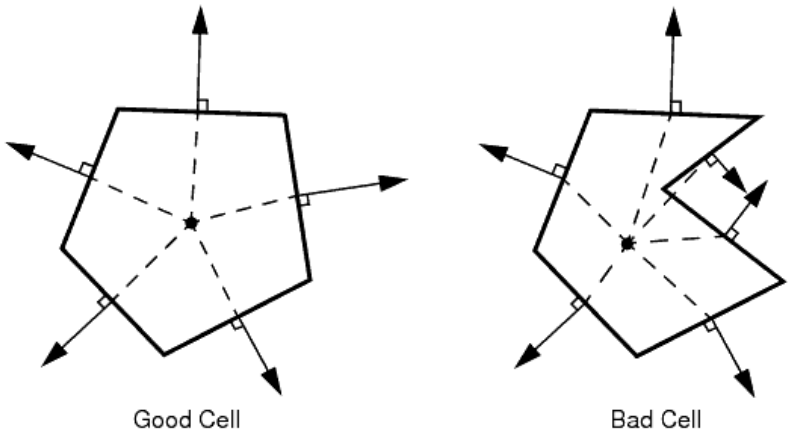

Figure 3.15 Examples of cells with differences in face validity (Siemens, 2018)

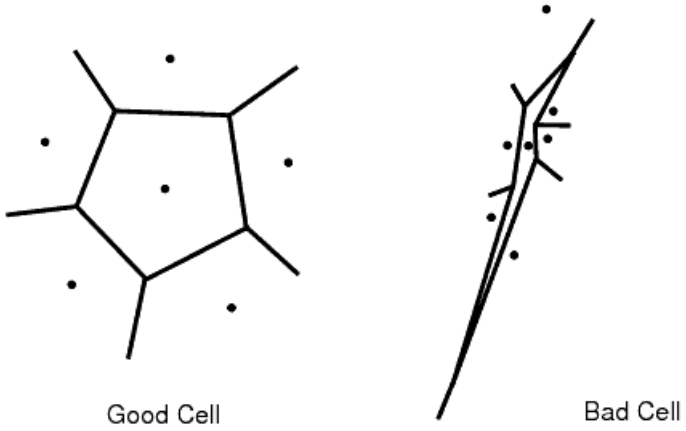

Figure 3.16 Cells with even and uneven geometric distributions (Siemens, 2018)

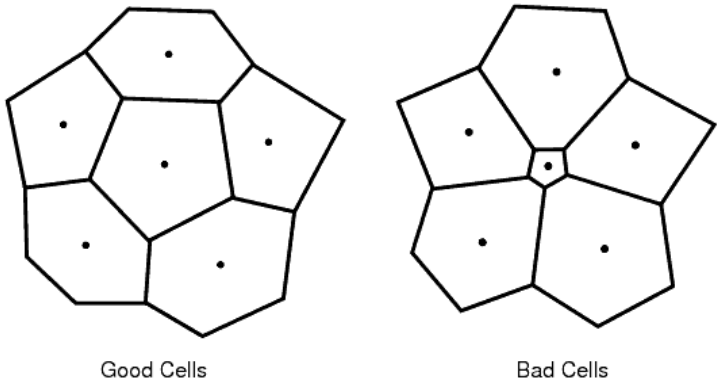

Figure 3.17 Examples of cells with even and uneven volumes (Siemens, 2018)

When running diagnostics on cells a score of 1.0 is an indicator of a perfect cell. The score for when a cell is considered bad varies by metric. The tables below show percentages of cells which are considered acceptable for a grid independent study.

Table 3.5 Grid quality test results for the liquid region

	Face Validity	Cell Quality	Volume Change
Percent of acceptable cells	100%	100%	100%

Table 3.6 Grid quality test results for the gaseous region

	Face Validity	Cell Quality	Volume Change
Percent of acceptable cells	100%	100%	100%

3.5 Liquid-Ullage Information Exchange

The liquid and gaseous portions of the flow in the cryostat are both dependent on each other. The boundary at the surface of the liquid argon will evaporate and cause mass to enter the gaseous region. Meanwhile, the energy required to vaporize the argon must be taken from surrounding liquid argon and will therefore cool the liquid down. The heat transfer at the surface can be mapped. The more information that a simulation has about the real operating conditions, the more accurate the solution can be. By using the solution of the liquid as a boundary condition for the gas, a more accurate answer can be found for the gaseous simulation. These simulations could be run simultaneously and by passing information to each other simultaneously, but running a dual phase simulation ends up taking more time and computational resources than the combined resources to run the

simulations individually. Single phase simulations can be run instead. When results have been collected that agree with experimental data, the boundary conditions can be applied to the other single phase simulation saving time and computational resources. Figure 3.18 shows where the information exchange between simulations will occur.

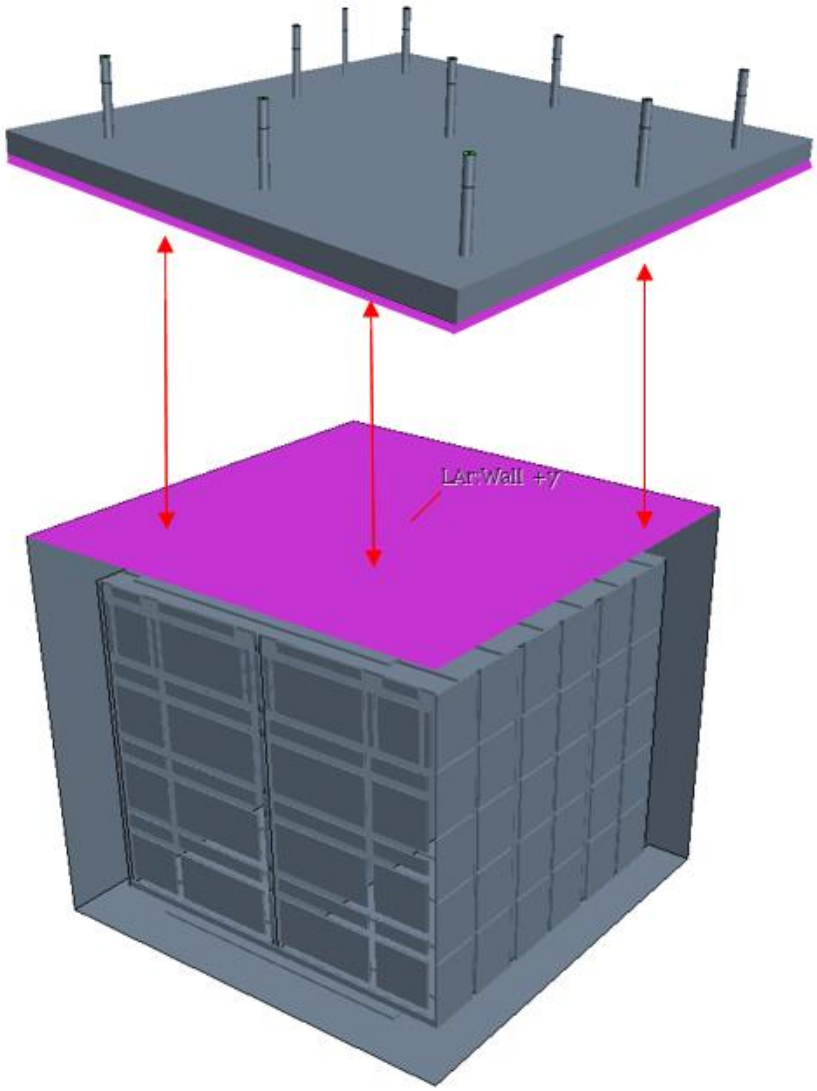

Figure 3.18 Boundary between two surfaces that need to share information

The amount of vapor that is being removed from the ullage is known. Therefore, the amount of mass that is entering is also known as the cryostat is in steady state. The

Figure 3.19 shows where the liquid argon is transferring heat at the boundary between the gas and the liquid.

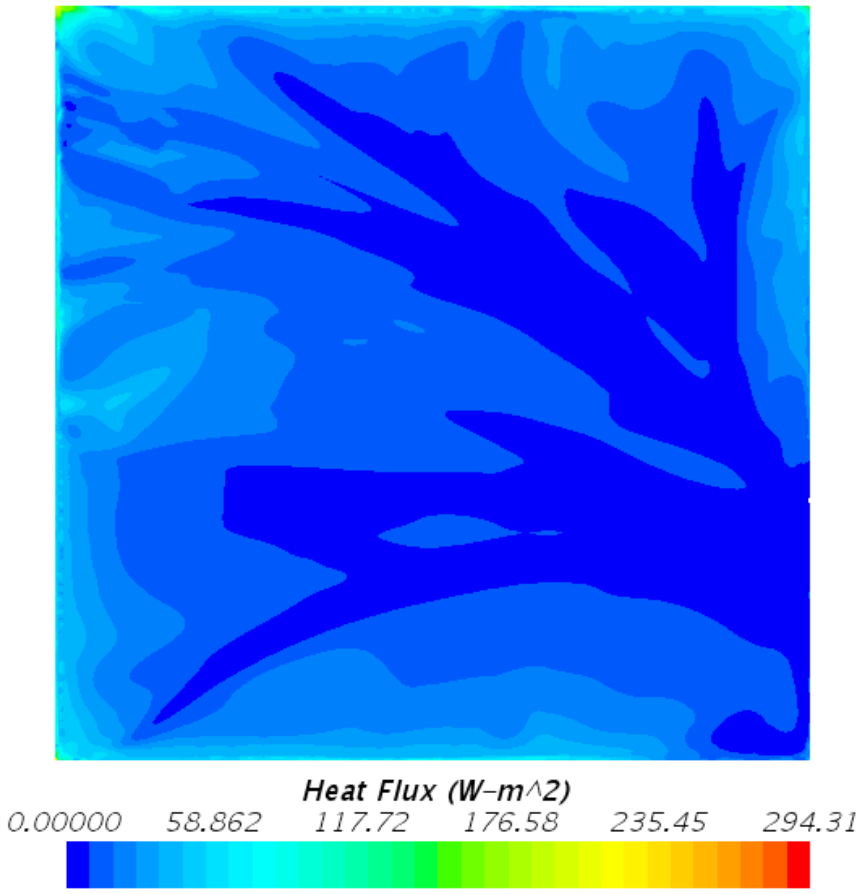

Figure 3.19 Cooling at the surface of the liquid argon due to boil-off

The liquid portion of the cryostat is being cooled at the surface due to the vaporization of argon. We have these areas of high argon vaporization mapped, we can vary the mass inlet in the ullage to reflect that there are some areas where there is a larger mass flux than others. A table is exported from Star-CCM+ into excel. In this table we can find the average heat flux on the surface. As the total mass flux at the inlet is already known, as is the area of the surface, we can also find the average mass flux on the surface. Then, a constant is found that makes the averages equivalent, and that same constant is applied to the roughly 60,000 data points exported into the CSV. Then, this

table is used as the mas flux input condition for the ullage. A simplified way to think about this method is shown below.

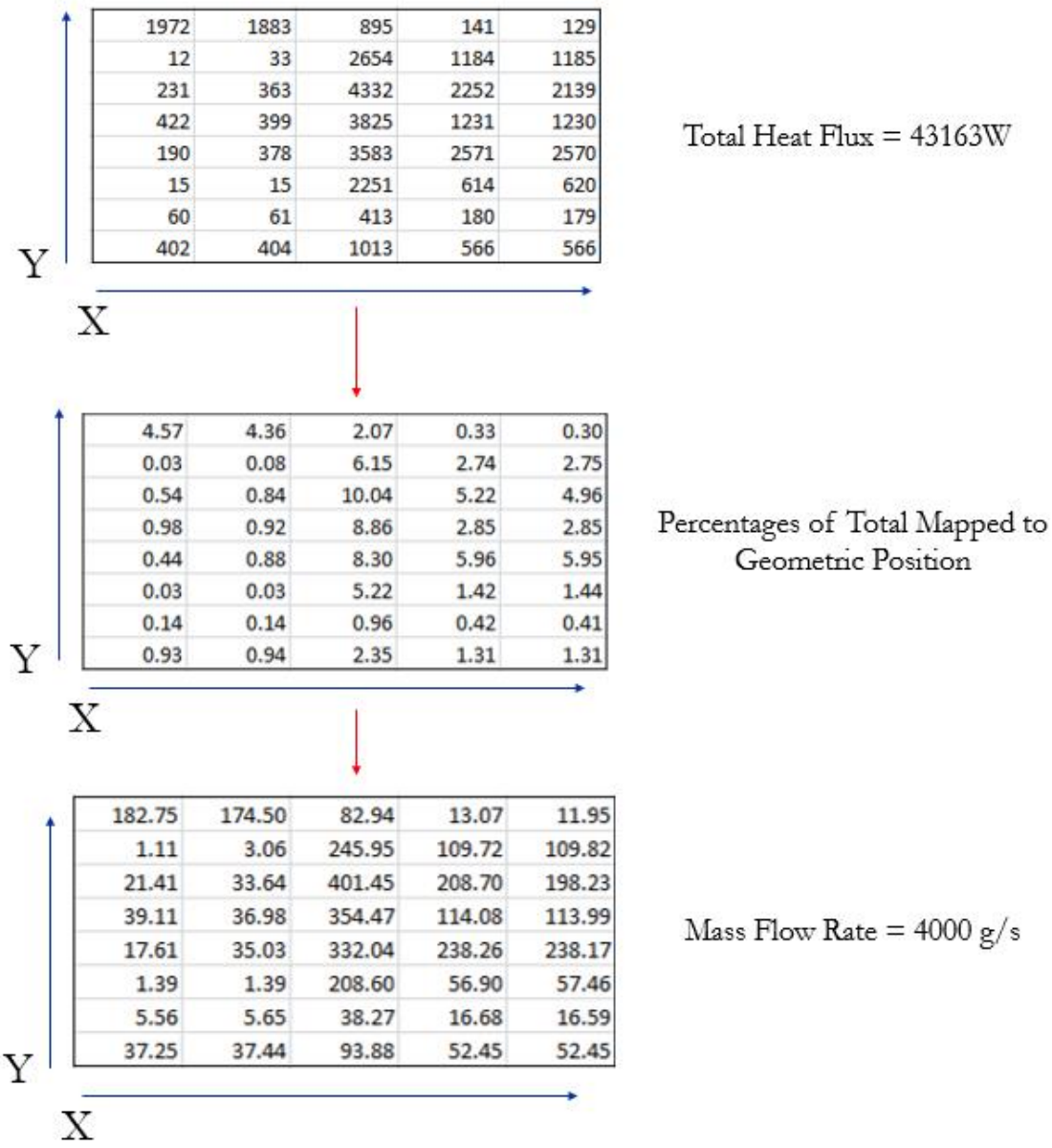

Figure 3.20 Mapping information from one simulation to another by creating a proportional grid for input

Expanding this procedure to the 60,000 data points exported from the CFD simulation of the fluid region gives Figure 3.21, showing the heat flux tabulated from the liquid portion next to the mass flux into the gaseous portion.

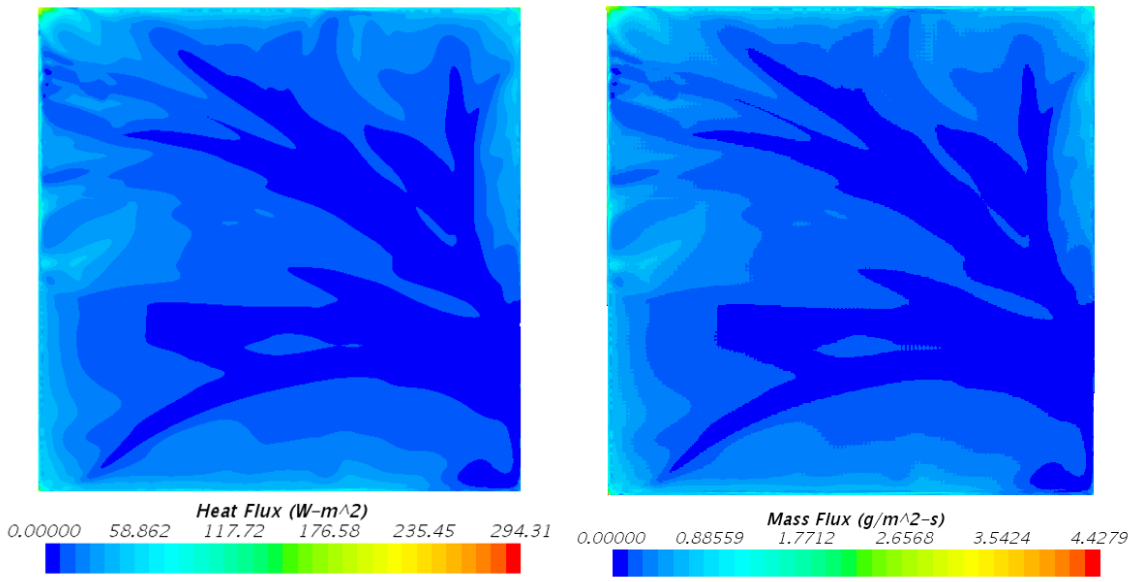

Figure 3.21 Heat flux (left) mapped to mass flux inlet (right)

4. RESULTS AND DISCUSSION

This chapter contains a report of the different simulations and how the boundary conditions had an effect on the solutions. It will start with discussion of the liquid region, comparing the static and dynamic temperature probe readings from the ProtoDUNE cryostat to the values that were found when running the simulation with different boundary conditions. This includes different simulations for different boundary conditions at the inlets and at the top surface of the liquid. The inlets will either have a mass flow rate (to signify when filtration is running) or have no mass flow rate (to signify when filtration is not running).At the top surface the shear condition will be looked at, as well as the thermal specification. With the simulation with the best boundary conditions chosen, an analysis of the flow profile inside the cryostat will be presented with regards to the purity of the liquid argon based on values detected by sensors in the physical cryostat. Using the purity of the cryostat, the lifetime for any free electrons in the cryostat can be found for any location inside the liquid region of the cryostat.

Next with the most accurate solution to the liquid region determined, the results of the ullage simulation can be covered in detail. The important topic to cover in the ullage is the propagation of impurities. There are two main factors involved in the propagation of impurities: the temperature profiles, due to the effect temperature has on the outgassing of impurities into the ullage, and the flow profiles, as the impurities can only reach the liquid if they propagate down from where they are created to the liquid surface.

An important area to look at is the effect of using the results of the liquid simulation on the flow of the ullage. If mapping the mass inlet of the ullage does not change the flow significantly, then it would not seem worthwhile to use this technique. If

it does change the simulation significantly, it should be used in future simulations to increase the accuracy of the solutions.

4.1 ProtoDUNE Single Phase Liquid Region

4.1.1 Comparison between CFD and ProtoDUNE Sensors

Data from the static temperature probe was collected from the four simulations with differences in thermal and shear boundary conditions placed at the top surface. The data collected from the experimental ProtoDUNE sensors were not calibrated absolutely. Therefore, the data from the simulations was scaled in such a way that the average temperatures of the experiment and CFD analysis would be equivalent. The data can then be compared by determining if the temperature profiles agree with each other.

The simulation using the slip and surface temperature boundary conditions at the surface of the liquid argon is shown in Figure 4.1.

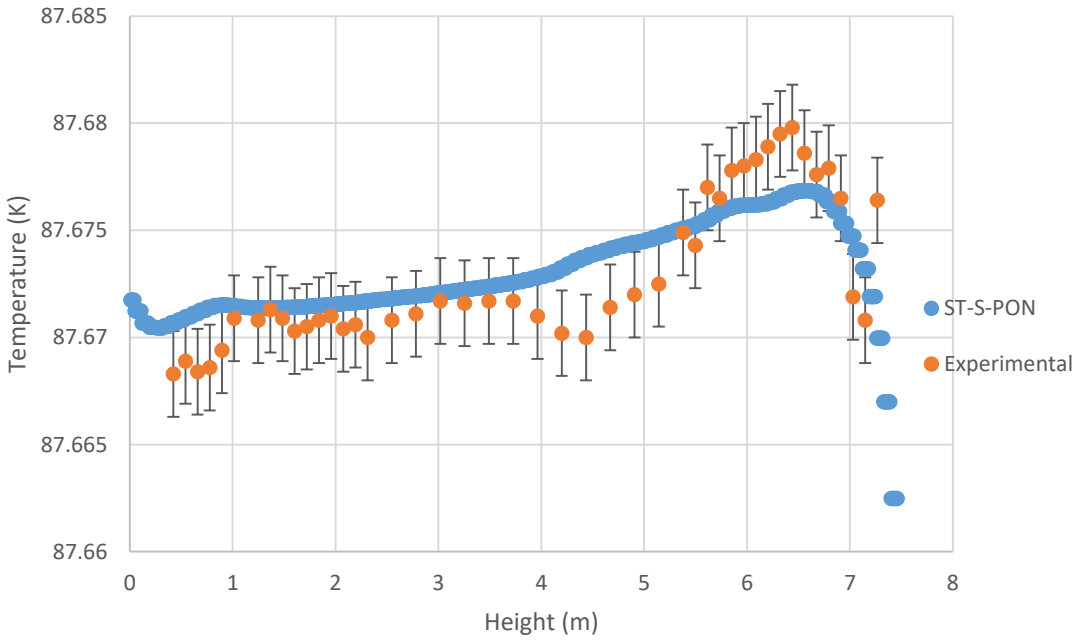

Figure 4.1 Surface Temperature, Slip, CFD Vs Experimental, Static Temperature Probe, Pumps On

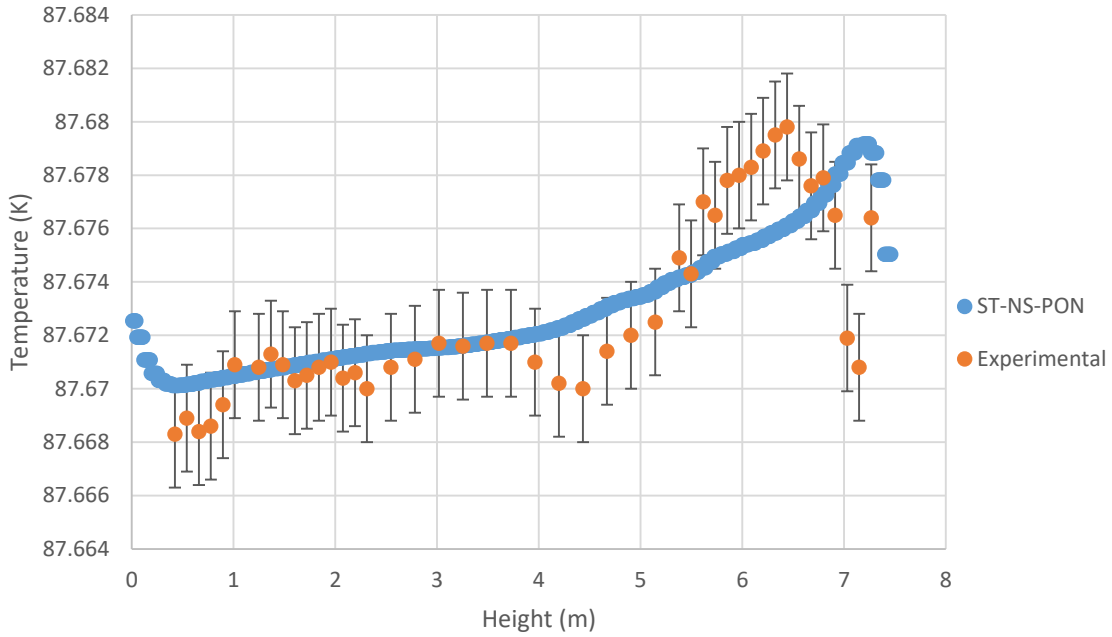

Figure 4.2 Surface Temperature, No-Slip, CFD Vs Experimental, Static Temperature Probe, Pumps On

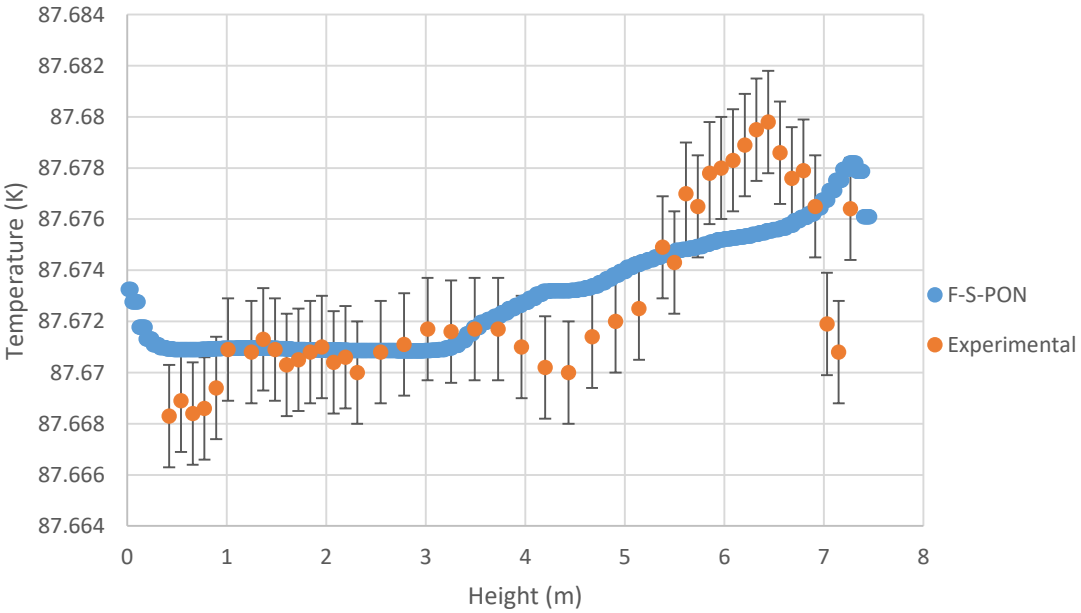

Figure 4.3 Heat Flux, Slip, CFD Vs Experimental, Static Temperature Probe, Pumps On

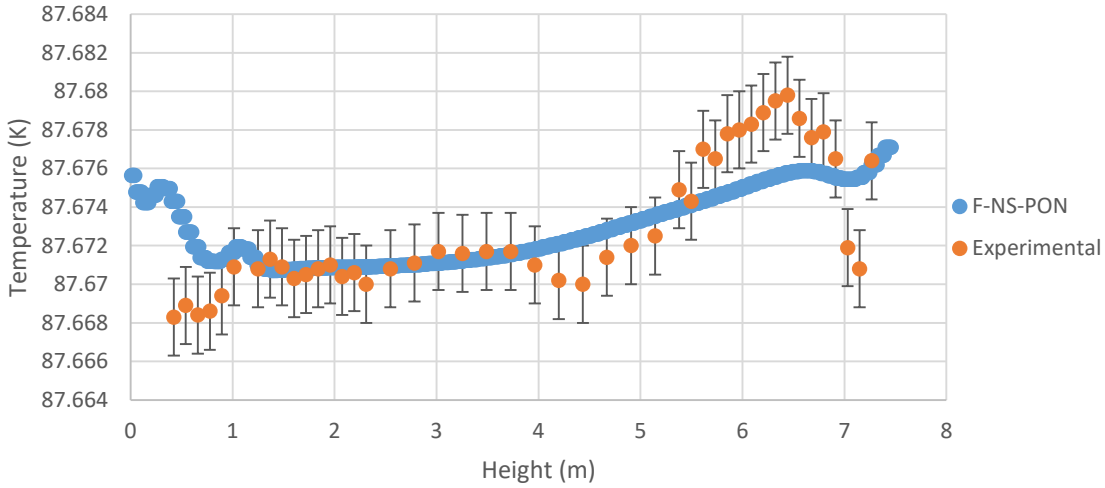

Figure 4.4 Heat Flux, No-Slip, CFD Vs Experimental, Static Temperature Probe, Pumps On

These graphs show a correlation between the height and the temperature in the cryostat. While none of them are perfect, they do show agreement between the simulations done at South Dakota State and the experimental data provided by Fermilab.

The dynamic temperature probe, located in the opposite corner of the static temperature probe, has similar results for the different boundary conditions.

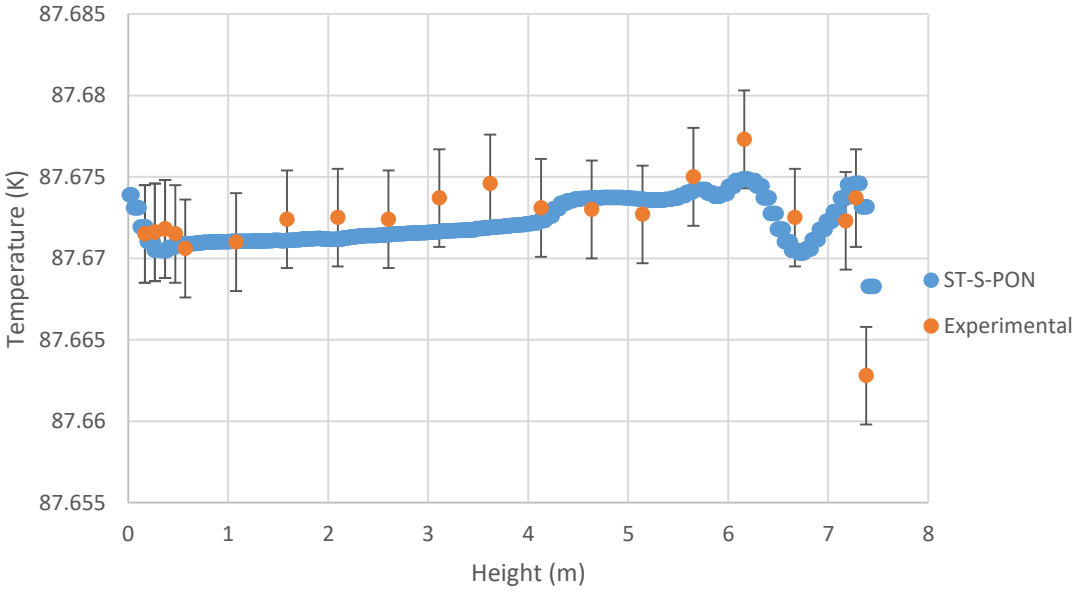

Figure 4.5 Surface Temperature, Slip, CFD Vs Experimental, Dynamic Temperature Probe, Pumps On

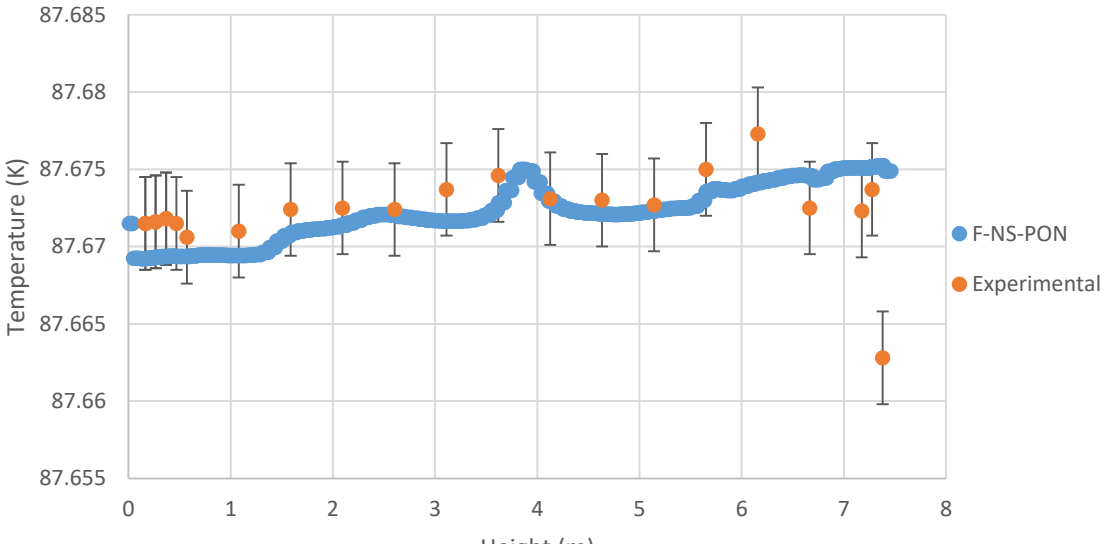

Figure 4.6 Surface Temperature, No-Slip, CFD Vs Experimental, Dynamic Temperature Probe, Pumps On

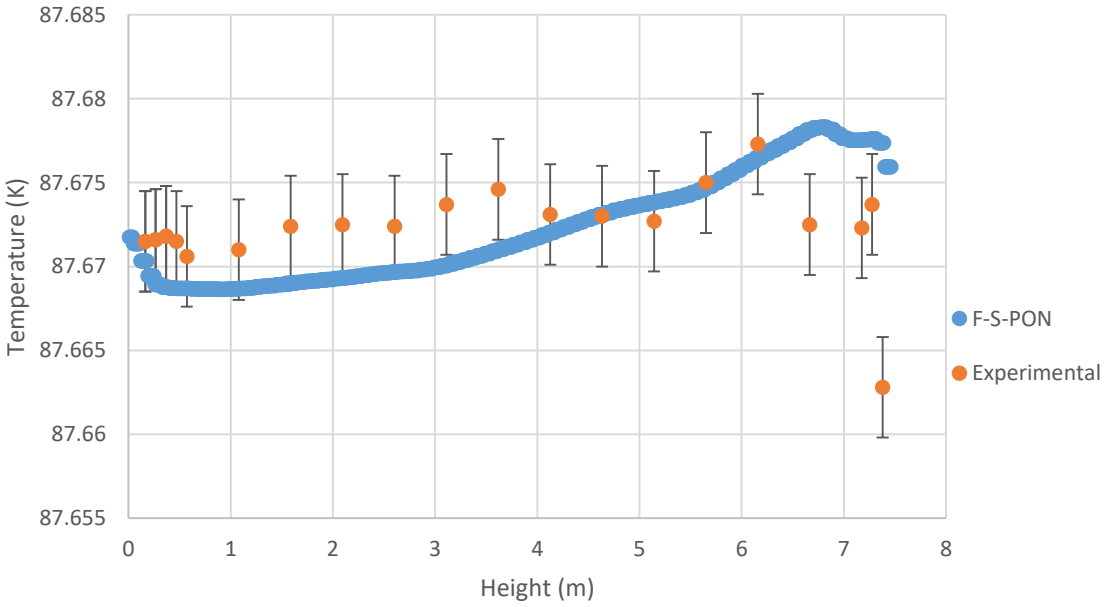

Figure 4.7 Heat Flux, Slip, CFD Vs Experimental, Dynamic Temperature Probe, Pumps On

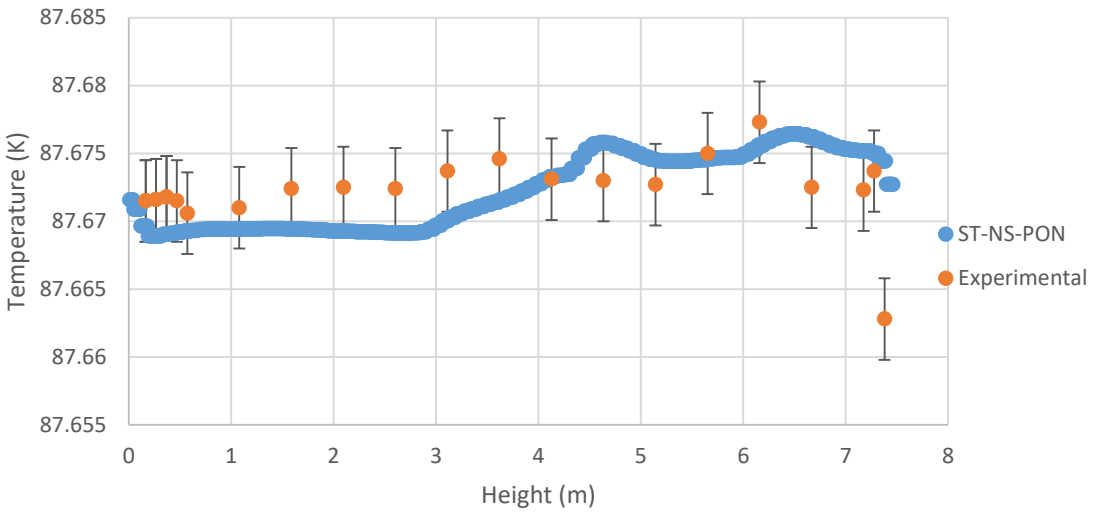

Figure 4.8 Surface Temperature, No-Slip, CFD Vs Experimental, Dynamic Temperature Probe, Pumps On

There is high level of agreement between the various boundary condition simulations and experimental data, especially from the simulation using a surface temperature and slip boundary condition, as well as the simulation using flux and no-slip boundary condition. These graphs are normalized to a common average. However, this does not detract from the point that almost all temperature readings are within the error bars of the data points, showing that the temperature trend is very strong.

Based on a visual inspection of the above graphs, the simulation with the surface temperature and slip boundary conditions appears to be the best combination to analyze for the ProtoDUNE single-phase detector. The mean squared error, which will be analyzed later, also supports this assertation.

Data was also collected from the ProtoDUNE Single-Phase cryostat while the pumps were turned off. It is important to note at this point that turning the pumps off changes the problem from a steady state problem to a transient one. Figure 4.7 shows the

average temperature of the cryostat during this period where the liquid argon pumps have been turned off.

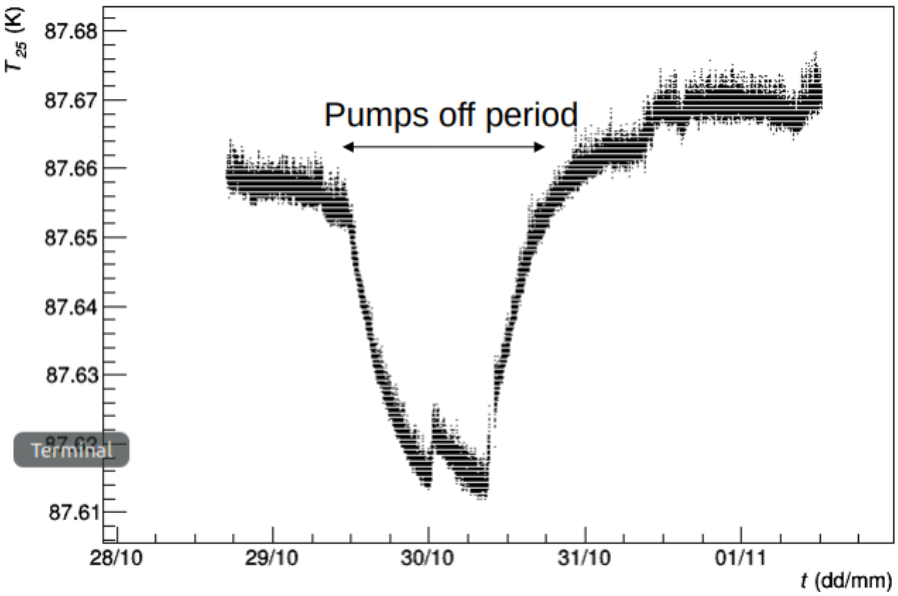

Figure 4.9 Average temperature of the cryostat while pumps are turned off (Garcia-Peris, 2019)

The average temperature during the liquid argon shutdown decreased. This is because while the pumps that return the liquid argon to the cryostat are not running, the pumps removing gas from the ullage remain in operation. This causes the temperature conditions at the surface to remain very similar to when the pumps are operating, but because the liquid argon is returned to the cryostat warmer than when it is pumped to the filtration system, turning off the pumps causes the average temperature of the cryostat to decrease.

CFD simulations were completed with the same boundary conditions as before but with the exception that the inlets would be turned off to see if the simulations could recreate the flow profiles that were found when the pumps were no longer running. The

temperature vs. height for the static temperature probe while the liquid argon return pumps are turned off is shown in Figures 4.10 – 4.13.

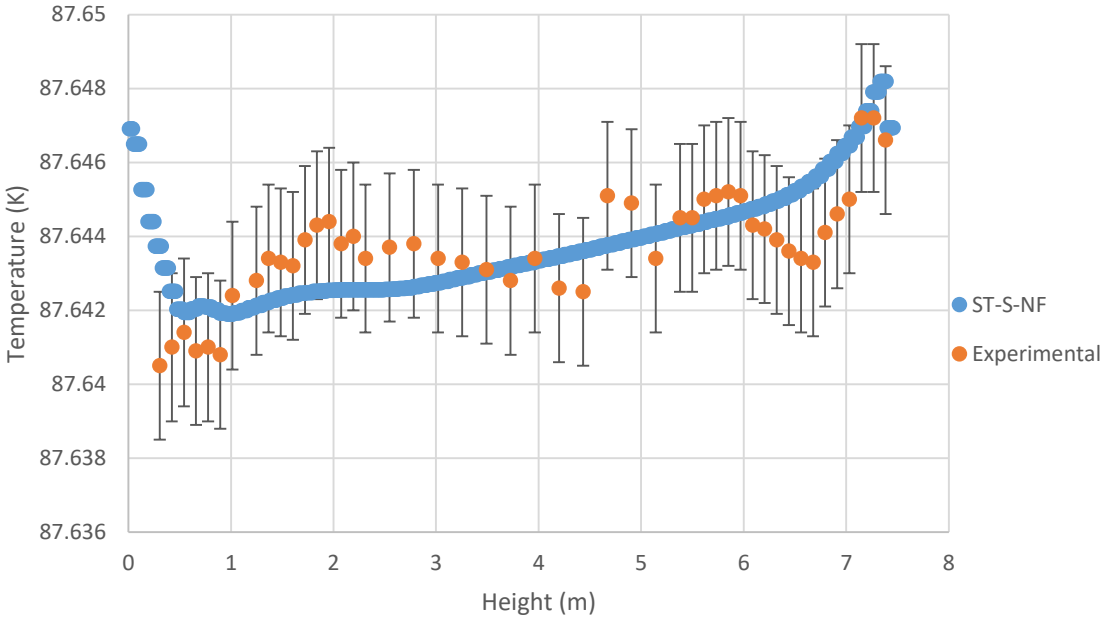

Figure 4.10 Surface Temperature, Slip, CFD Vs Experimental, Static Temperature Probe, Pumps Off

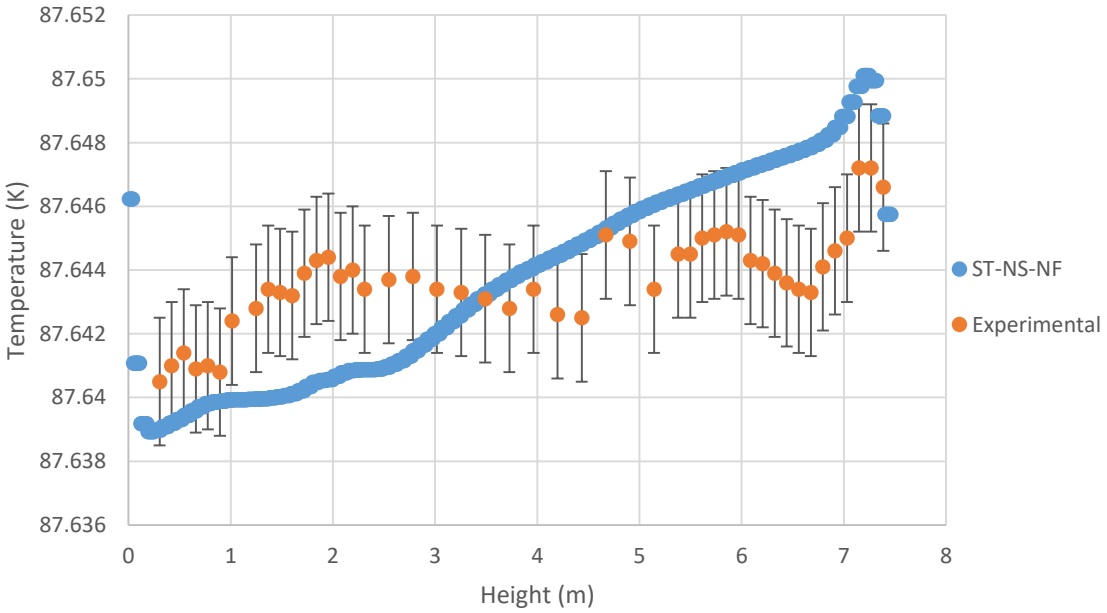

Figure 4.11 Surface Temperature, No-Slip, CFD Vs Experimental, Static Temperature Probe, Pumps Off

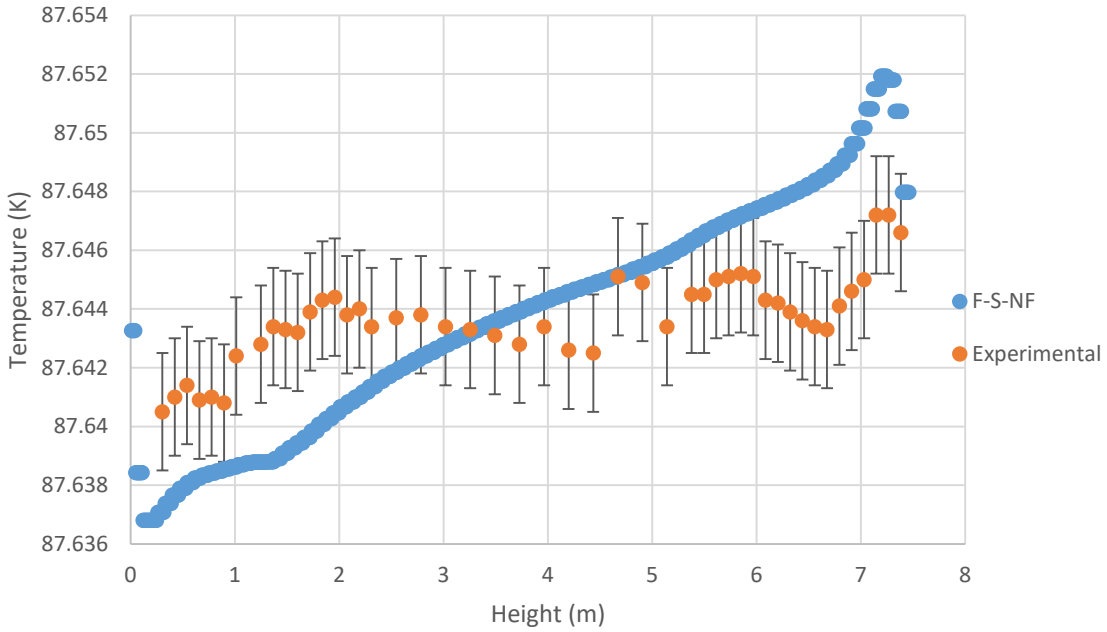

Figure 4.12 Heat Flux, Slip, CFD Vs Experimental, Static Temperature Probe, Pumps Off

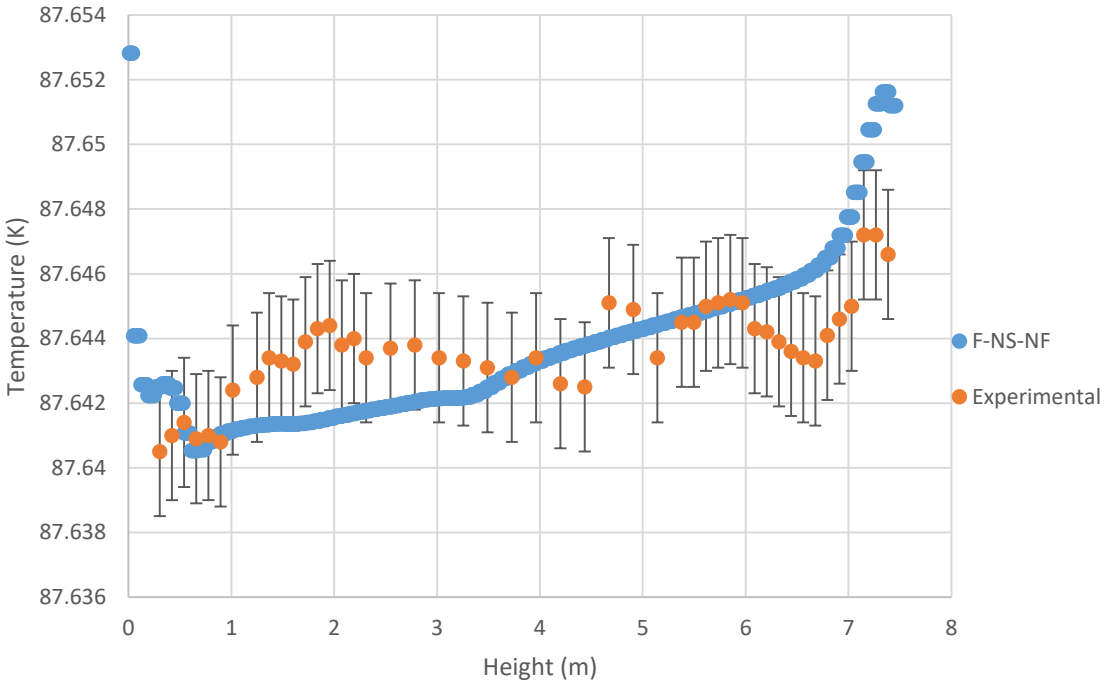

Figure 4.13 Heat Flux, No-Slip, CFD Vs Experimental, Static Temperature Probe, Pumps Off

The figures above show that in the case of the static temperature probe, simply changing the inlet condition may not be the best way to analyze this flow. Each graph of CFD results shows a fairly linear regression for temperature as the height of the probe increases, while experimental data seems to show a lot more variability and non-linearity. The data collected from the same pump shutdown but for the dynamic temperature probe is shown in Figures 4.14 – 4.17.

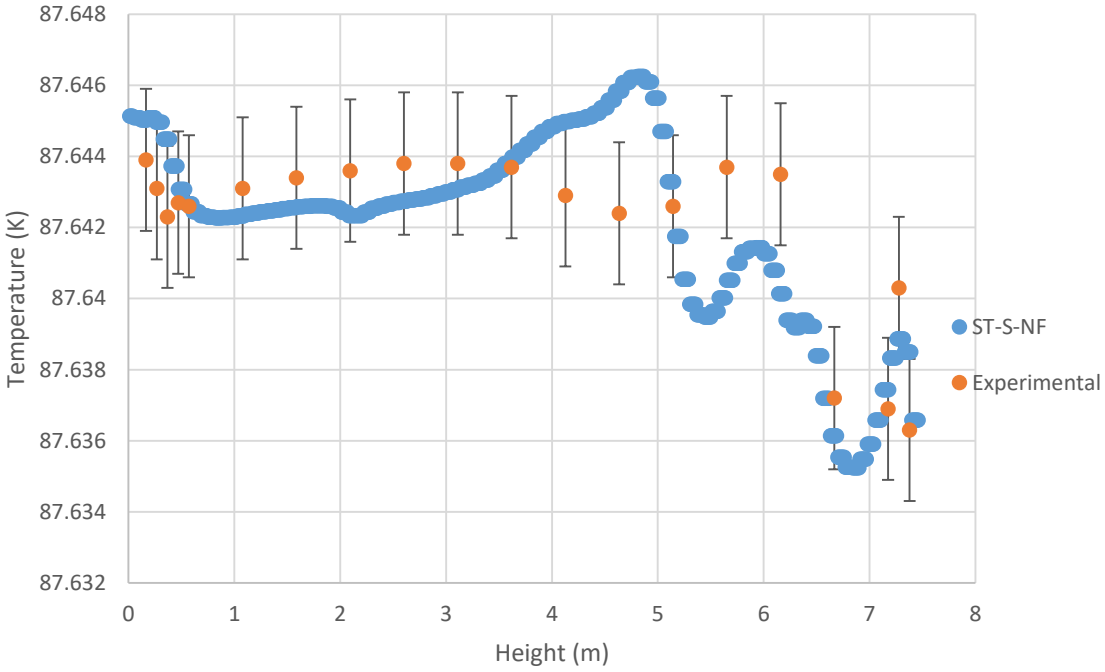

Figure 4.14 Surface Temperature, Slip, CFD Vs Experimental, Dynamic Temperature Probe, Pumps Off

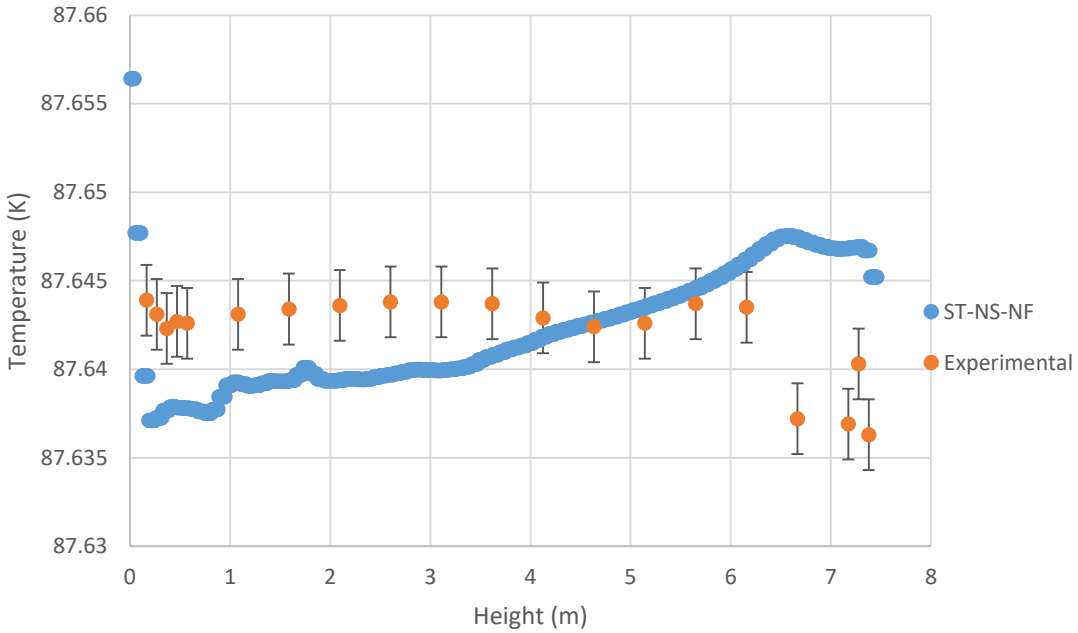

Figure 4.15 Surface Temperature, No-Slip, CFD Vs Experimental, Dynamic Temperature Probe, Pumps Off

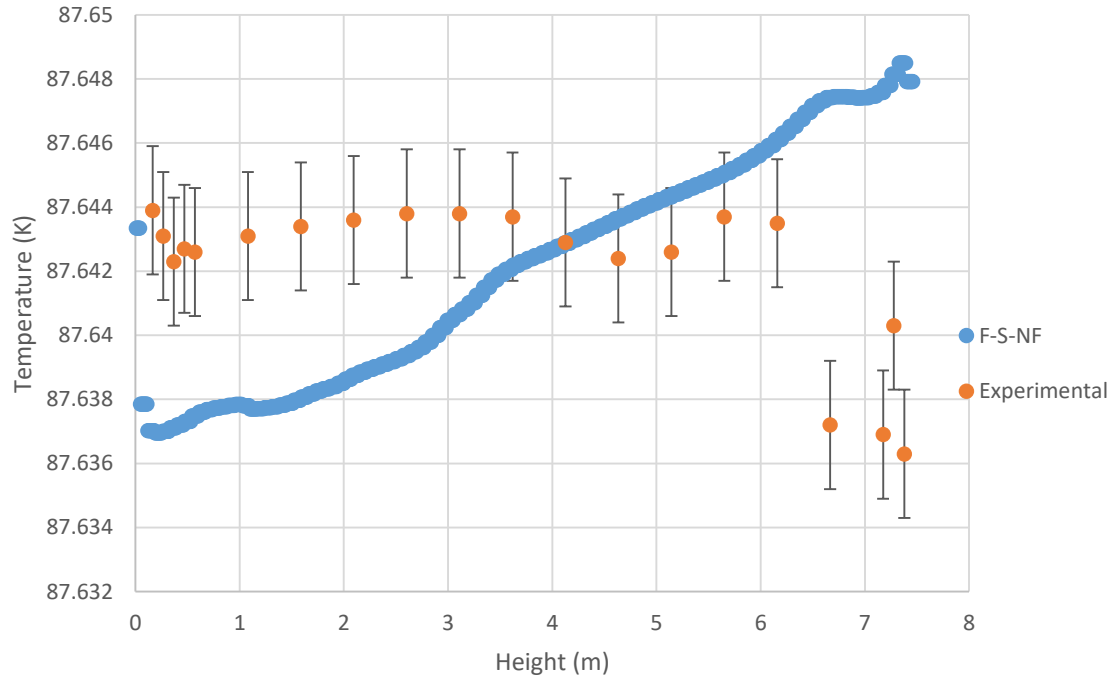

Figure 4.16 Heat Flux, Slip, CFD Vs Experimental, Dynamic Temperature Probe, Pumps Off

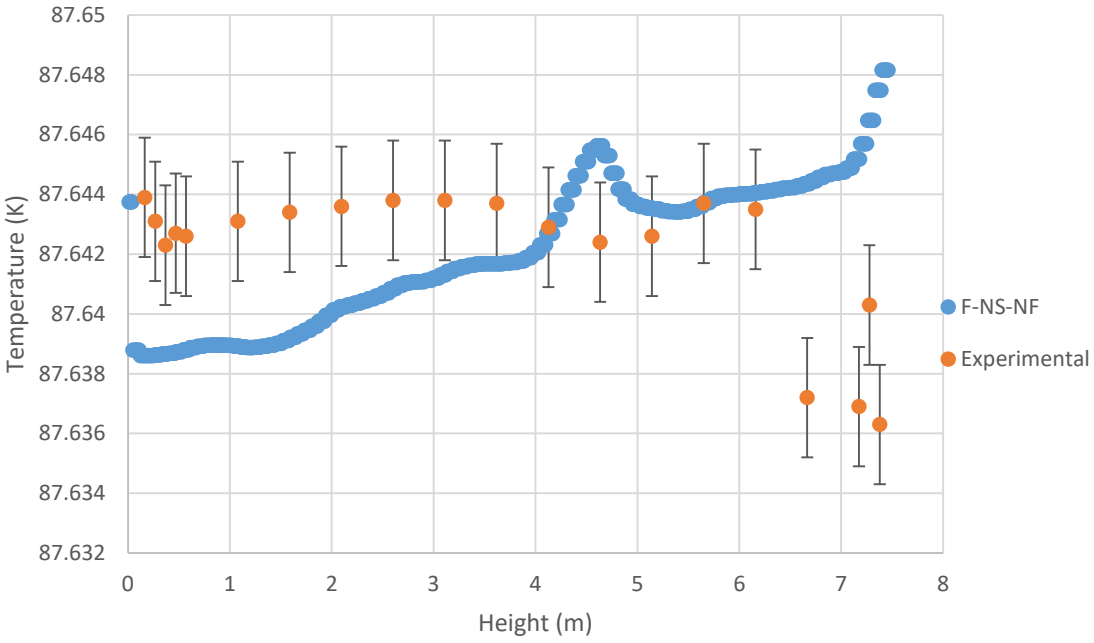

Figure 4.17 Heat Flux, No-Slip, CFD Vs Experimental, Dynamic Temperature Probe, Pumps Off

As was the case with the static temperature probe, there are not a lot of similarities between the profiles of the experimental and simulation data. The simulation data has again been scaled in order to properly compare the profiles. Table 4.1 shows the temperature correction for each simulation for the averages between the simulation and experimental data to be equal. Table 4.2 shows the mean squared error for the different boundary conditions.

Table 4.1 Temperature correction amounts based on probe type and boundary condition

	Static Temperature Probe				Dynamic Temperature Probe			
	Surface Temperature		Heat Flux		Surface Temperature		Heat Flux	
	Slip	No-Slip	Slip	No-Slip	Slip	No-Slip	Slip	No-Slip
Pump On	-0.061	0.454	0.293	1.011	-0.062	0.454	0.292	1.01
Pump Off	-0.014	0.566	0.308	0.984	-0.008	0.568	0.311	0.987

Table 4.2 Mean squared error $*10^6$ based on probe type and boundary conditions after correcting for average

	Static Temperature Probe				Dynamic Temperature Probe			
	Surface Temperature		Heat Flux		Surface Temperature		Heat Flux	
	Slip	No-Slip	Slip	No-Slip	Slip	No-Slip	Slip	No-Slip
Pump On	4.09	5.14	5.05	5.02	1.61	5.44	7.67	2.89
Pump Off	1.18	7.21	10.44	2.98	1.27	12.29	14.88	9.31

The surface temperature and slip boundary condition pairing above is by far the lowest correction factor for both the static and dynamic temperature probes. This, as well as the mean squared error of the simulation temperature profiles in comparison to the experimental data leads to the conclusion that this is the best set of boundary conditions to simulate the ProtoDUNE single-phase detector.

4.1.2 CFD Results

The flow regime will be analyzed using the CFD results from the simulation with the constant surface temperature and slip boundary conditions as these are the most accurate based on temperature profile and absolute difference between the readings from the experiment and the simulations.

Temperature profiles with velocity vectors super imposed give a good idea of how, in general, the warm liquid argon tends to move towards the surface. This flow is reduced in areas where the APA planes and field cage are present as they provide both viscous and inertial resistance.

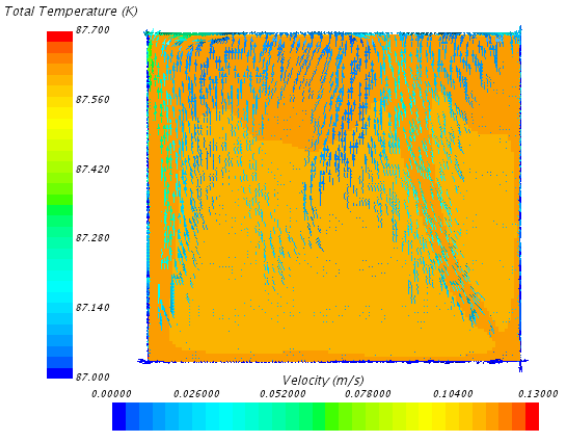

Figure 4.21 Cross section of cryostat at x=-4.1 m

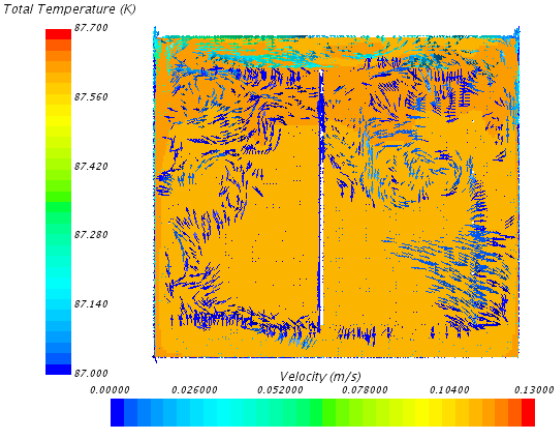

Figure 4.20 Cross section of cryostat at x=-3.0 m

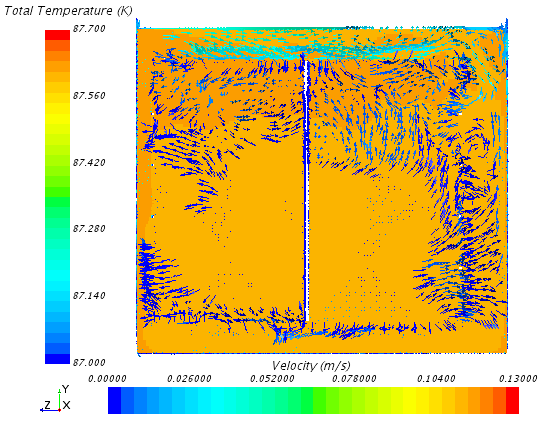

Figure 4.18 Cross section of cryostat at x=-2.0 m

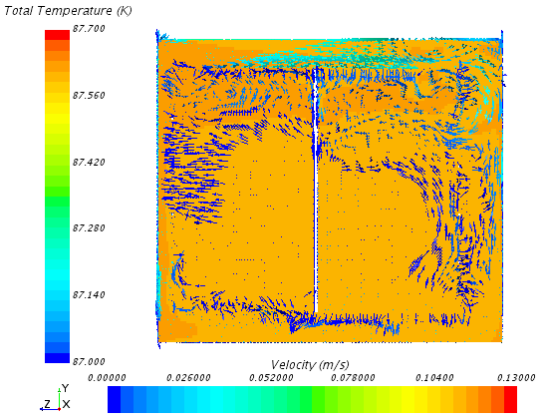

Figure 4.19 Cross section of cryostat at x=-1.2 m

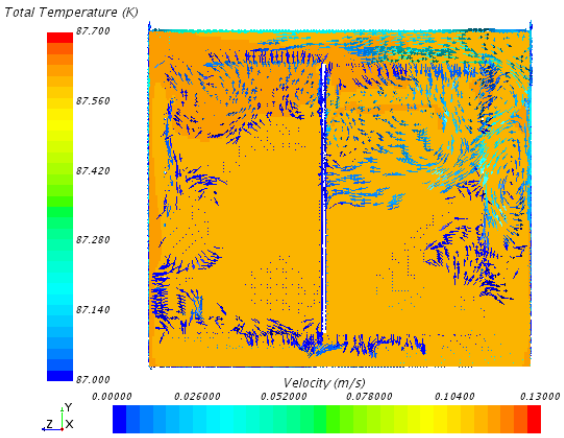

Figure 4.23 Cross section of cryostat at x=0.0 m

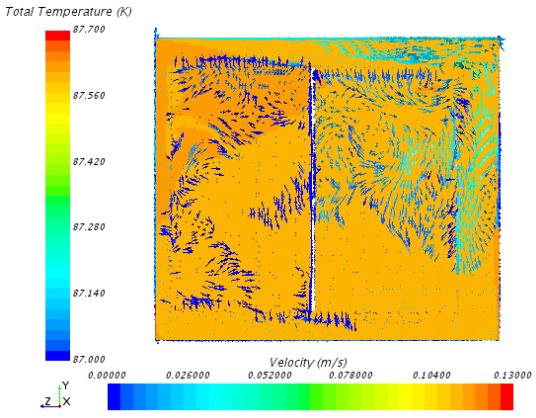

Figure 4.22 Cross section of cryostat at x=1.2 m

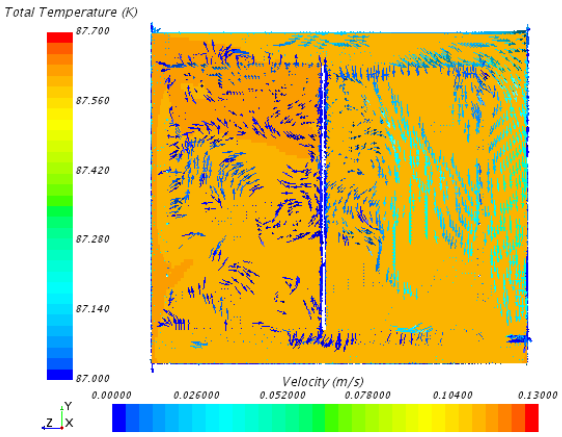

Figure 4.27 Cross section of cryostat at x=2.0 m

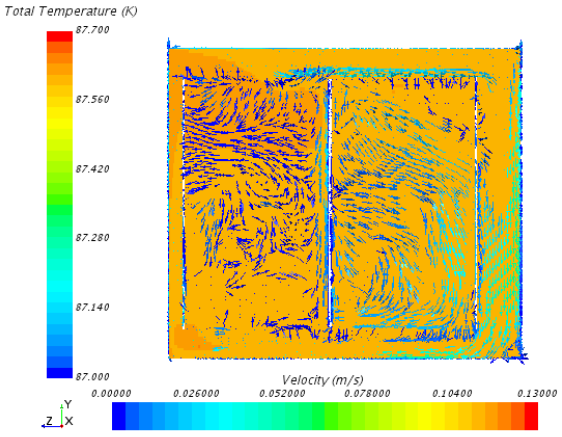

Figure 4.26 Cross section of cryostat at x=3.0 m

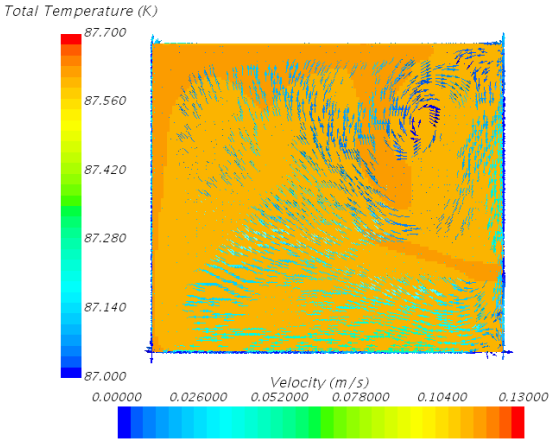

Figure 4.25 Cross section of cryostat at x=4.1 m

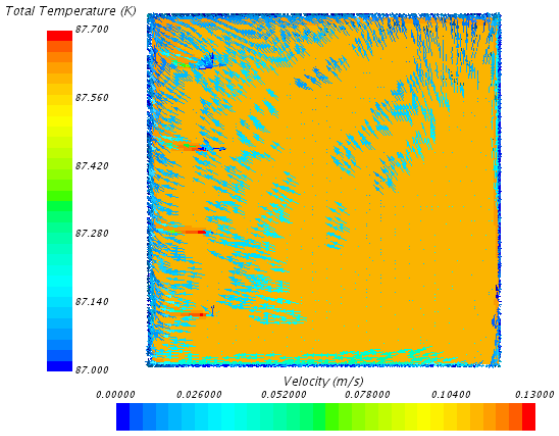

Figure 4.24 Cross section of warm argon inlets

Temperatures are relatively homogenous throughout the cryostat. They generally do not change more than 0.01 K. In fact, taking the minimum and maximum temperature in the simulation gives a temperature difference of 0.0245 K at the most extreme. As natural convection is the main driver of the fluid flow, accurate temperature mapping is important for the accuracy of the flow because the Boussinesq approximation is calculating the buoyant forces. An isometric view of the cryostat with streamlines originating from the inlets shows fluid motion inside the cryostat. These are provided in figure 4.28

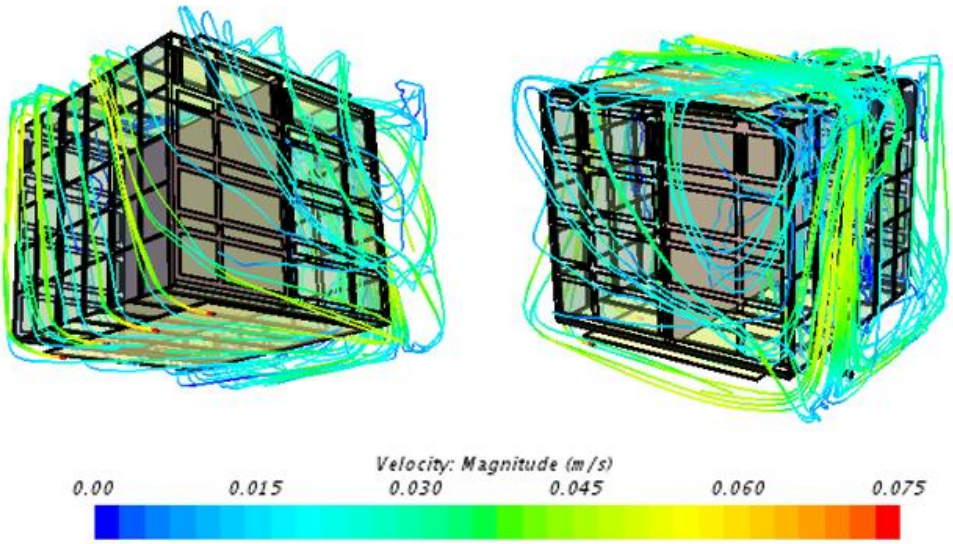

Figure 4.28 Streamlines of fluid velocity in the liquid portion of the cryostat

Visual representation of flow using streamlines are helpful for understanding the flow in the cryostat. The streamlines for the case where there is no flow into the cryostat from the filtration pumps can be seen in Figure 4.29

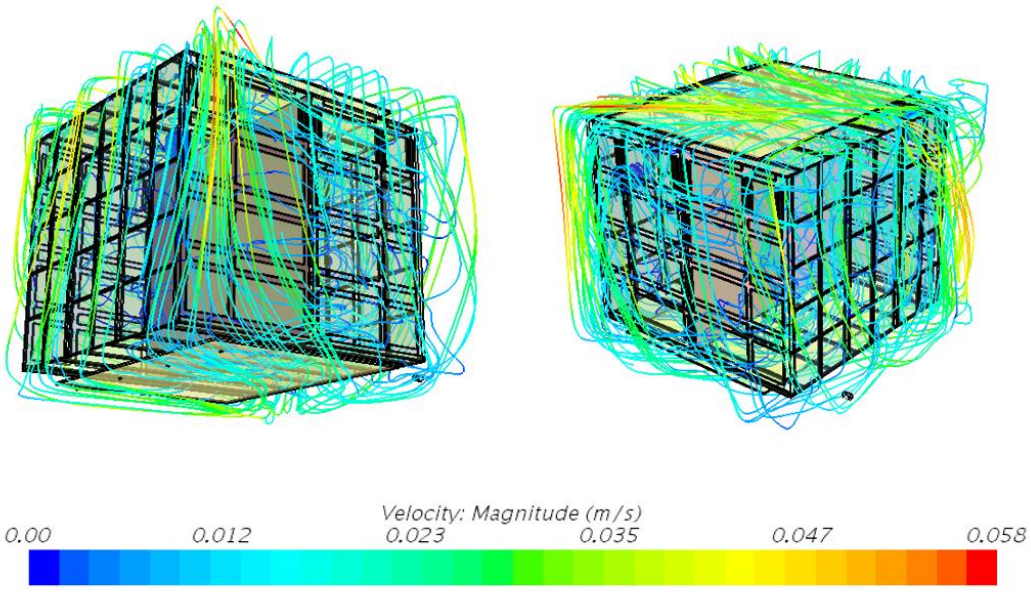

Figure 4.29 Streamlines of fluid velocity in the liquid portion of the cryostat when filtration is off

Ultimately the goal was to make sure there is an adequate amount of mixing in the cryostat. With good flow and lots of fluid movement, researchers make sure that impurities in the cryostat would move around a lot and become homogenous so as not to skew the detection results. If almost all the impurities were in one half of the cryostat, it would appear as if something incredibly strange were occurring when collecting neutrino data. The amount of impurities in the cryostat is inversely related to how long the electrons knocked off the argon atoms can remain free in the fluid. This means that we are looking for two things in our simulations for impurity. We want low levels of impurity overall, and we want the impurities to be even distributed throughout the detector.

Total impurities can be calculated based on the outgassing and interaction with warm cables entering the cryostat. Outgassing happens primarily in the ullage and then the impurities filter down into the liquid argon from the ullage. Using sensor data provided by Fermilab, a simulation can be run using an arbitrary impurity flux modeled as a passive scalar. Real levels of impurities at any location in the simulation can be found by using a proportion between known impurity data at a specific point and simulated impurity data at that same point.

Figure 4.30 was created by finding the average level of impurities in the cryostat per unit volume, then finding the minimum and maximum and dividing by the average.

These values are then graphed per iteration to see how the minimum and maximum change as the simulation settles on a solution.

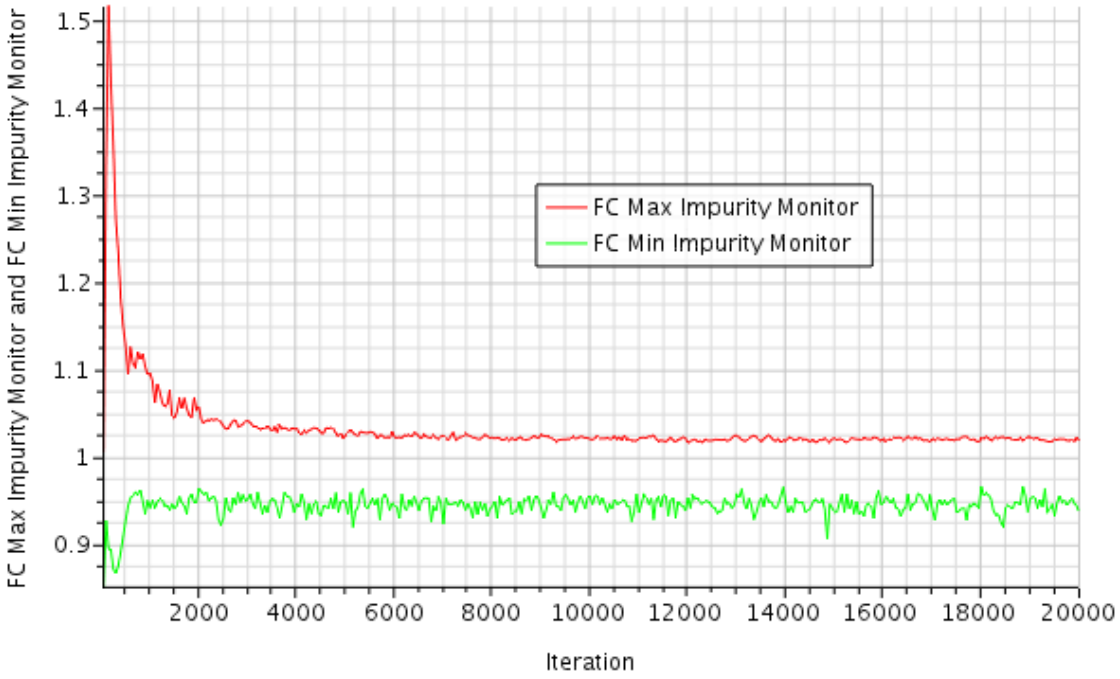

Figure 4.30 Minimum and maximum impurities per unit volume scaled to an average of one.

Figure 4.30 shows that there is good homogeneity throughout the cryostat with no areas getting much higher or lower than the average, but researchers at Fermilab also want to know absolute values. This can be done by taking the impurity levels measured experimentally in the cryostat and scaling the impurities in the simulation based on that point. The impurity data is scaled from the data in Figure 4.31 given to SDSU to help with our research.

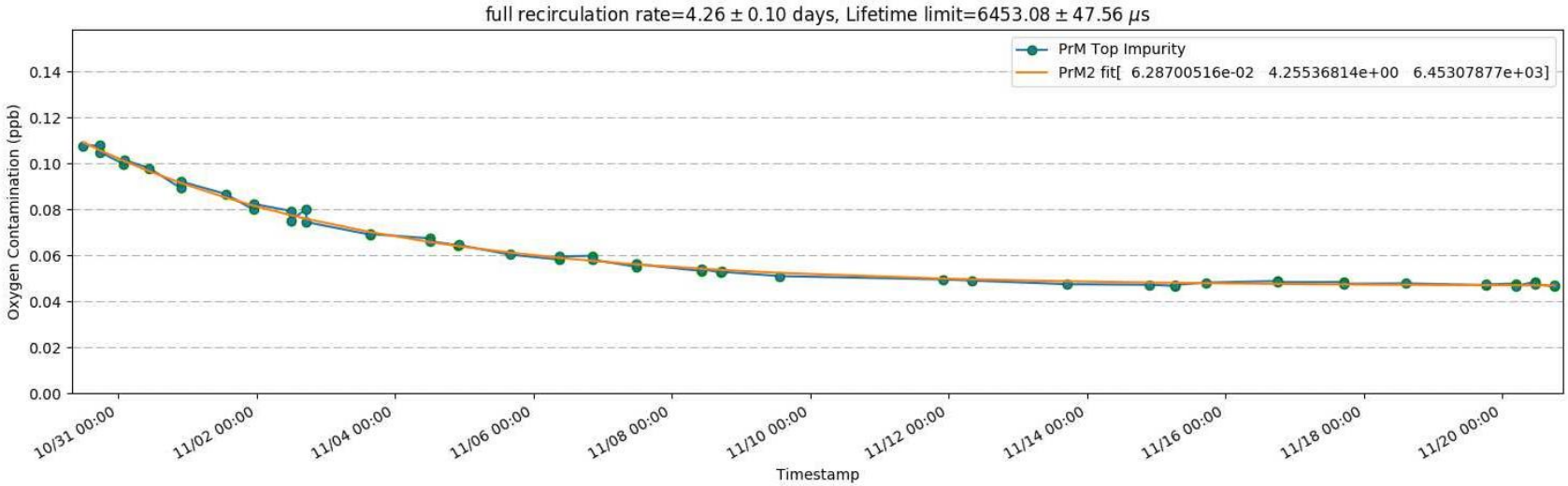

Figure 4.31 Impurity data collected by Fermilab of the ProtoDUNE cryostat

With the absolute amount known for a single location, it is easy to find that the minimum amount of oxygen in the cryostat is 0 ppb (This is due to the assumption of pure liquid argon entering from the filtration system) and the maximum 0.064 ppb. This may go down further as the cryostat continues to be filtered.

Figure 4.32 shows the levels of impurity at a given cross-section through the TPC. A study conducted in the TPC, where it is most important to have pure argon, has a maximum impurity level of 0.0512 parts per billion.

The grey bar in the middle of Figure 4.32 is an area of solid stainless steel and not argon, therefore impermeable to the flow of argon and impurities

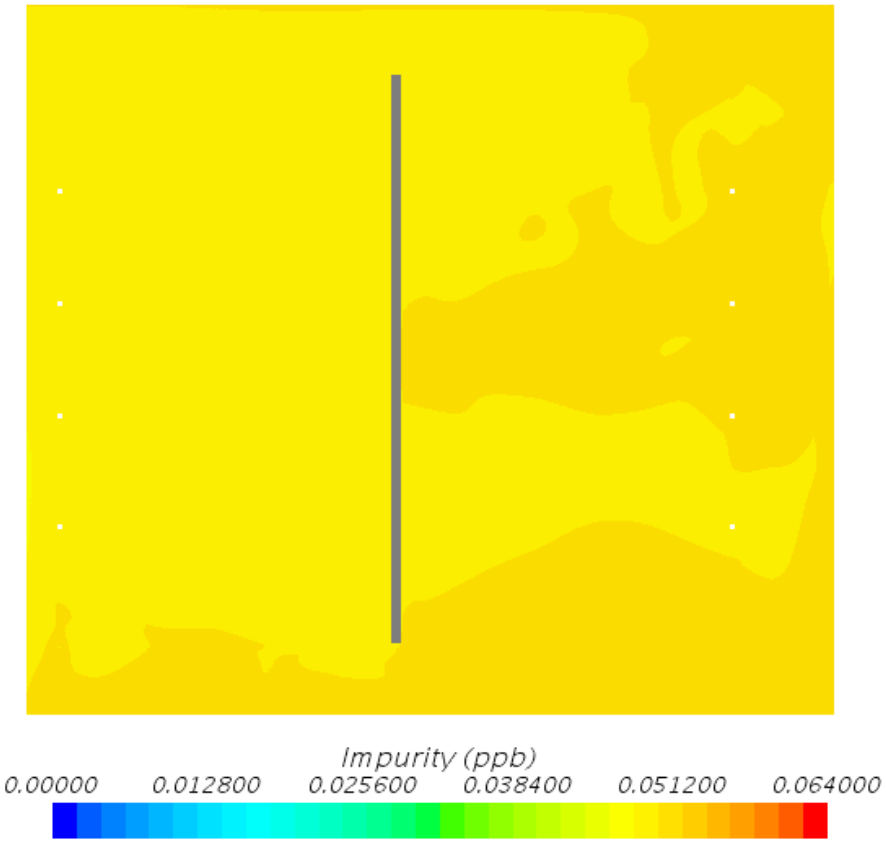

Figure 4.32 Impurity levels at the cross-section x=0.0m

Figure 4.33 shows how the perfect purity of the argon entering the inlets reduces the absolute impurities to zero in the areas near the inlet. In reality, there will still probably be small levels of impurity entering after the filtration system, but it would be small in comparison to the level of impurity in the cryostat.

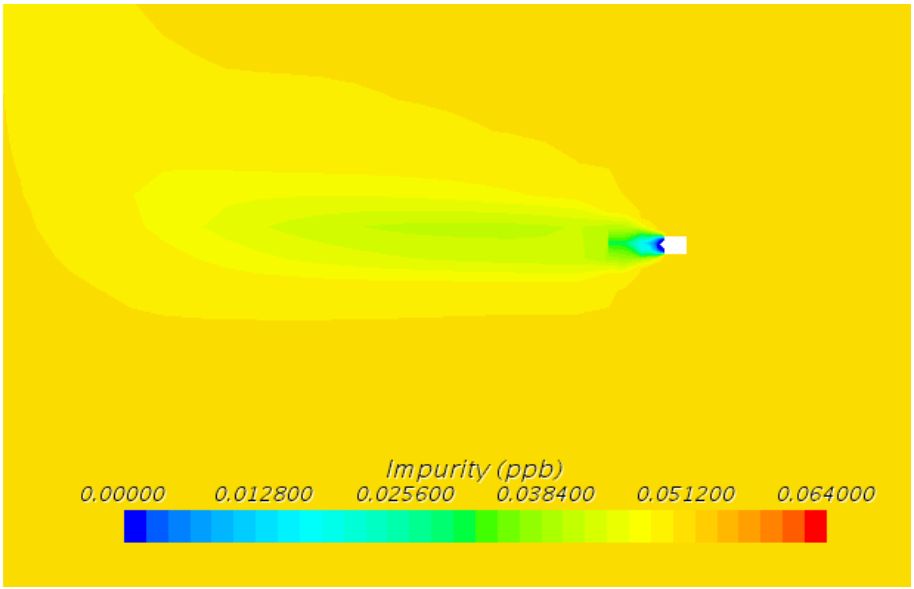

Figure 4.33 Cross-section of argon inlet with perfect purity.

The number of impurities in the cryostat are inversely proportional to the lifetime of any free electrons separated from the argon by neutrinos. It is important to have an idea of how long the electrons can last inside the detector because it takes a certain amount of time for the electrons to reach the data acquisition equipment. If the electrons are being absorbed before reaching the equipment, no measurements can be taken. The guidelines set out by researchers state that the maximum drift time of an electron is 2.25 ms, they have also stated that the detector must meet a purity level so as to allow for an electron lifetime greater than 3 ms. The simulations completed for this thesis found the average electron lifetime due to oxygen impurity in the cryostat to be 5.98 ms. Looking again at

the TPC where the lifetime is most important gives an average of 6.0 ms. A cross section of the detector shows the electron lifetime in Figure 4.34.

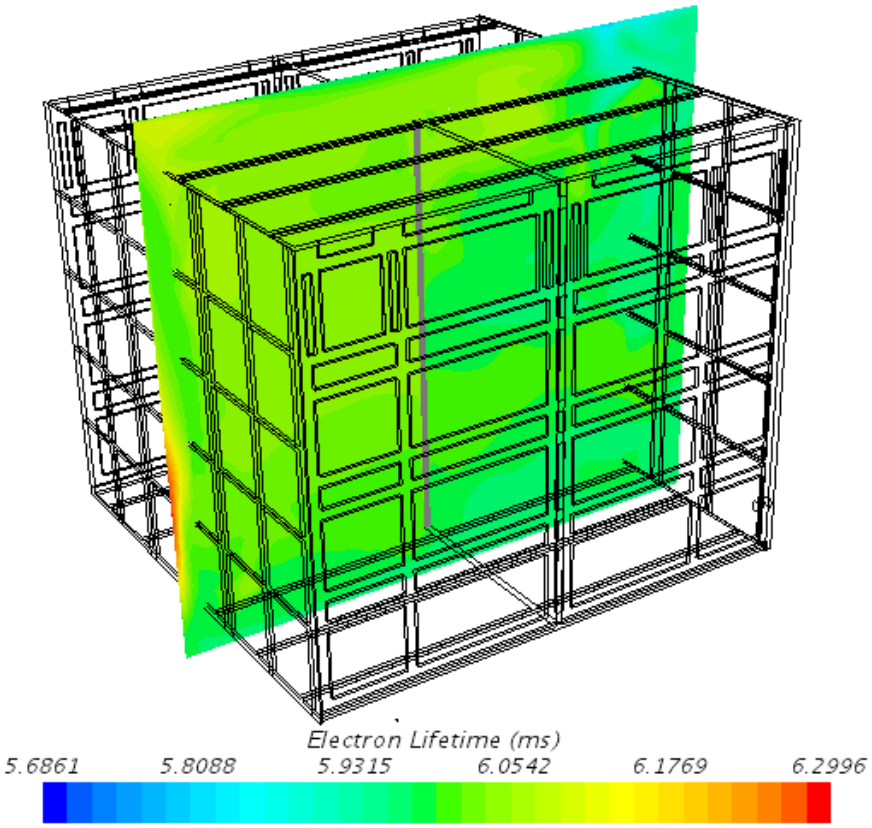

Figure 4.34 Electron lifetime in the detector and cryostat.

4.2 ProtoDUNE Single Phase Ullage Space

The gaseous portion of the Single-Phase ProtoDUNE cryostat does not have the same amount of sensors that are in the liquid region. In this region, data can be collected from the CFD simulations, but cannot be verified with experimental data from the cryostat. All sensors need wires that penetrate the cryostat. There wires, or more specifically, the Teflon insulation around these wires, are where the impurities enter the cryostat. The amount at which the Teflon outgasses is a function of temperature, a graph of outgassing can be seen in Figure 4.35.

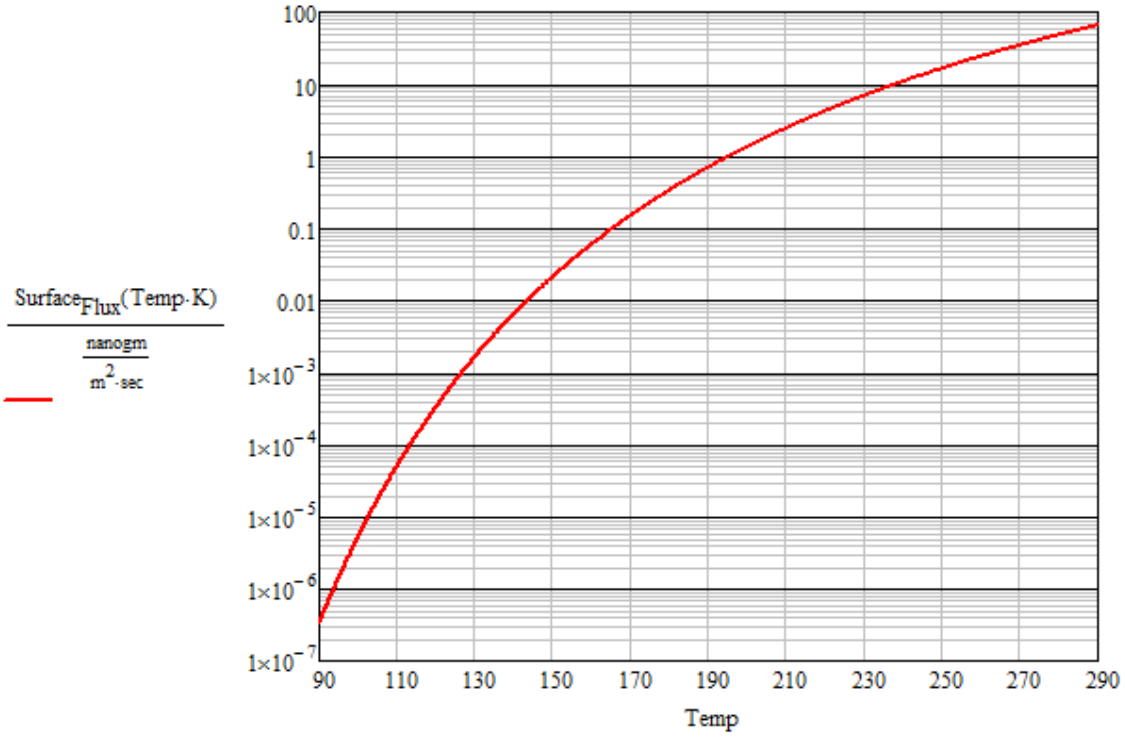

Figure 4.35 Outgassing as a function of temperature for Teflon wire insulation.

The ullage is not a long term priority to monitor temperature or impurities, therefore, sensors are not included in this area. The dynamic temperature probe could enter this area, but in doing so would become contaminated and increase impurities to the liquid upon its return.

A cross section view of the ullage temperature profile is shown in Figure 4.3The

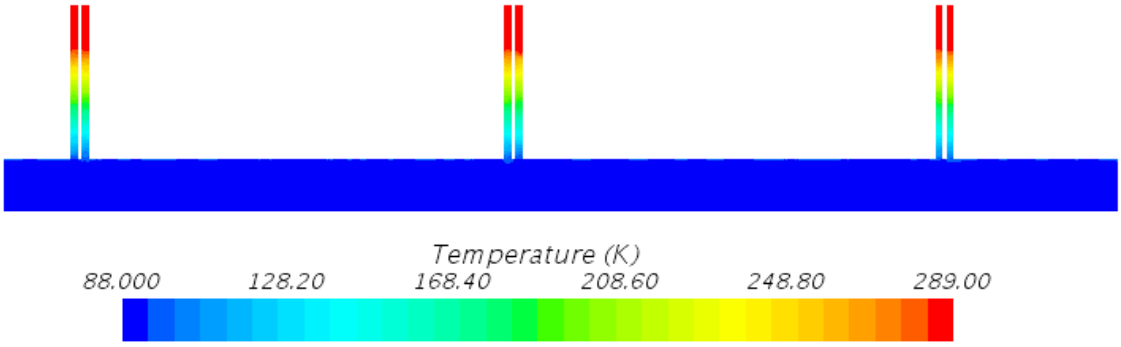

Figure 4.36 Temperature profile of ullage.

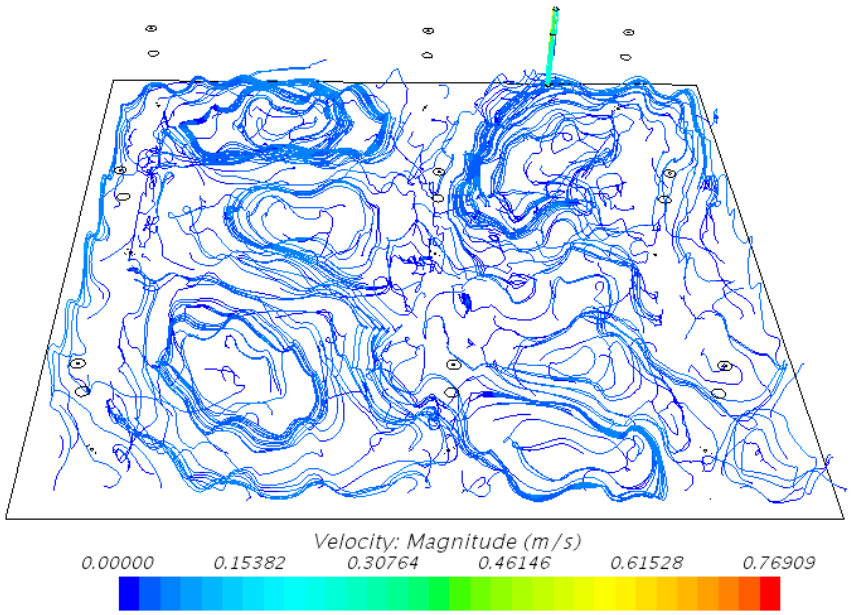

Figure 4.37 Isometric view of streamlines derived in the ullage

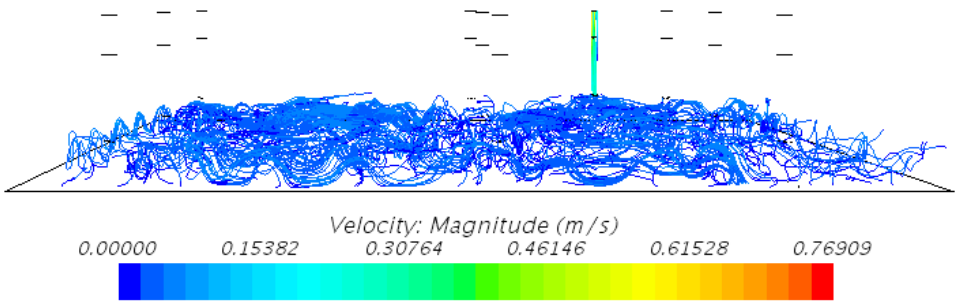

Figure 4.38 Side view of streamlines derived in the ullage

temperature distribution is one that does not support large amounts of natural convection.

In general, the higher temperatures are at the top and the lower temperatures are at the bottom. Density decreases as temperature increases so the more dense fluid will be located at the bottom of the ullage which means natural convection will not cause mixing in this flow. Streamlines for this flow can be seen in Figure 4.37. The side view of this shows that the fluid does not move much in elevation unless it's being evacuated from the chamber.

4.3 Liquid Ullage Information Exchange Effects

When changing the mass inlet from a uniform inlet to an inlet based on the heat transfer of the ullage, changes are easily identifiable, but it is import to distinguish whether these differences are significant. Figures 4.39 and 4.40 show the same viewing angles as 4.37 and 4.38 above.

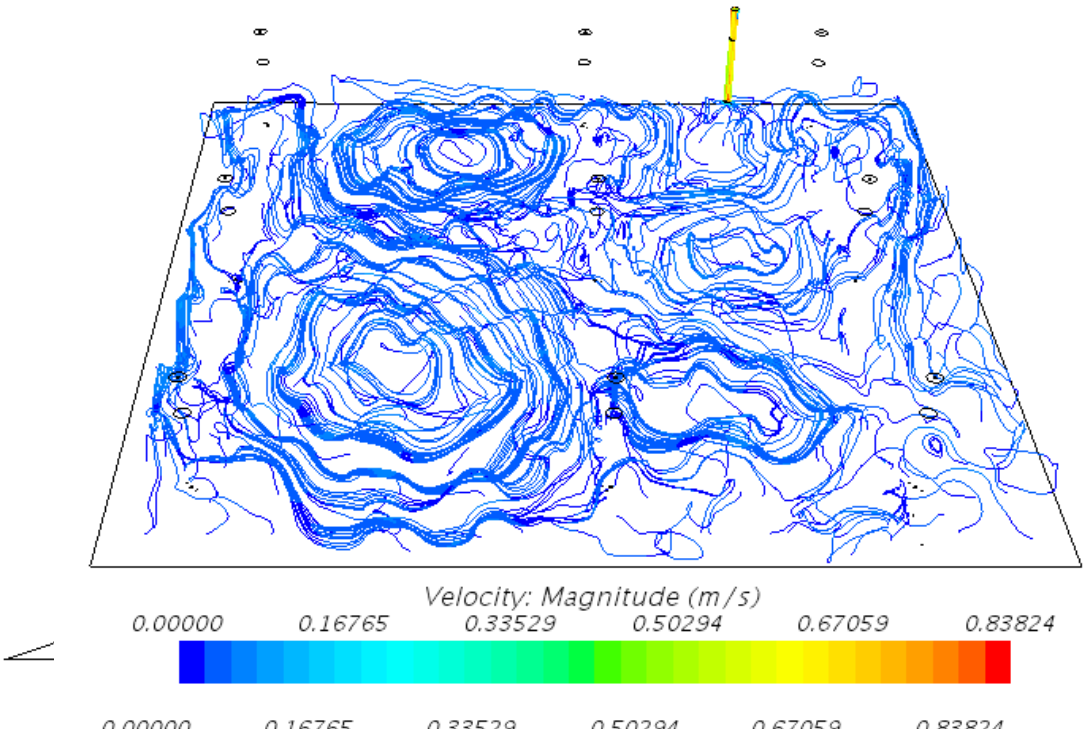

Figure 4.39 Isometric view of streamlines derived in the ullage with a variable mass inlet
Figure 4.40 Side view of streamlines derived in the ullage with a variable mass inlet

The same amount of streamlines were created in both the simulations, so the only difference between the two is the how flow has been influenced by the change in boundary conditions. With natural convection having much less effect on the total motion of the fluid, it makes sense that varying the inlet velocity has a large effect on the total fluid motion, indicated by the significant change in streamlines from Figures 4.37 and 4.38 to Figures 4.39 and 4.40. This mixing lowers the total mass of impurities in the ullage almost an order of magnitude from about 0.73 kg to 0.087 kg. The concentration of impurities is more homogenous as well, as can be seen in Figures 4.41 and 4.42.

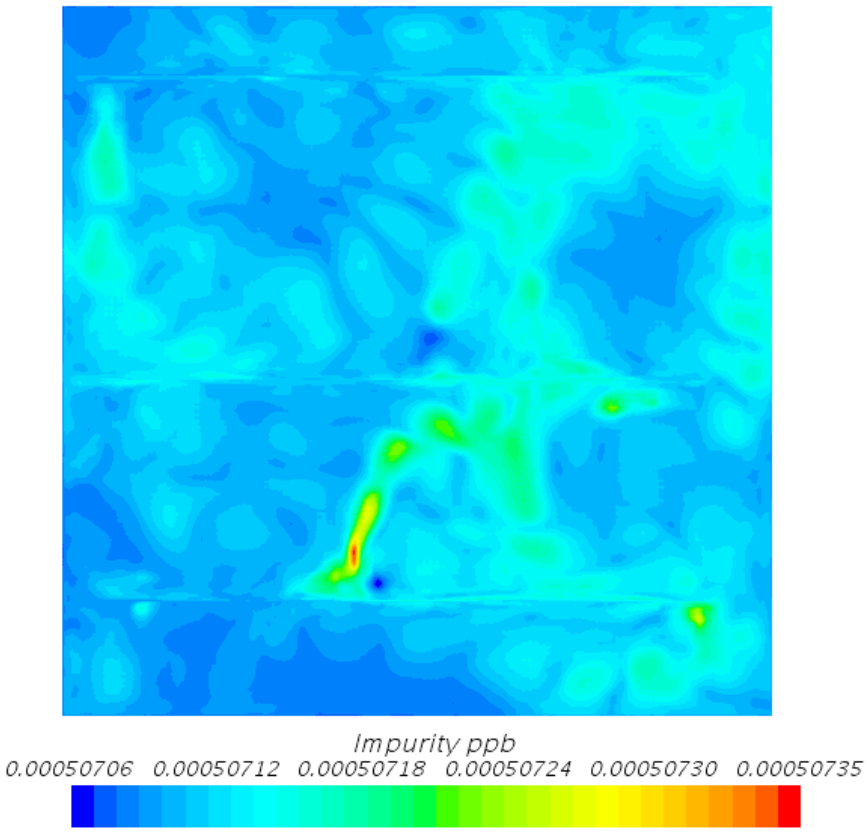

Figure 4.41 Impurity concentration 5cm above the inlet, variable inlet

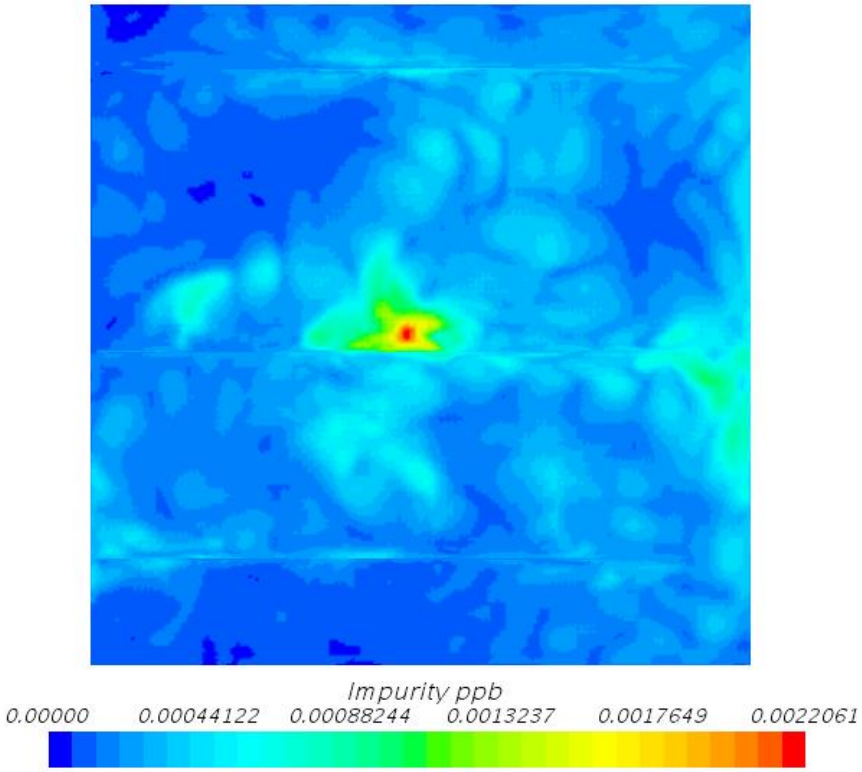

Figure 4.42 Impurity concentration 5cm above the inlet, constant inlet

Although difficult to see by just looking at streamline or temperature profiles, the reduction of impurities in the ullage by an order of magnitude shows clearly that having more boundary condition information is important to the accuracy of the results attained from the simulations.

This information was also very important to the Fermilab researchers. With the results of the ullage simulation known, it was theorized that the purity of the liquid detector could be improved by changing the outgassing procedure of the ullage. All of the cryostat penetrations are equipped with a gaseous purge that connects to the filtration system, the amount each chimney is drawing gaseous argon can be controlled and all excess argon being pumped out through a dedicated gaseous argon return. In order to determine the best mode of operation, a simulation was run where instead of a majority

(99%) of argon was being drawn out of the main return and a minority (1%) being drawn across the nine cryostat penetrations, the inverse would be true. With each chimney having 11% of the total amount of argon leaving, it was hoped that this would significantly lower the amount of impurities that could potential filter down into the detector. The streamlines for this simulation look significantly different than past simulations.

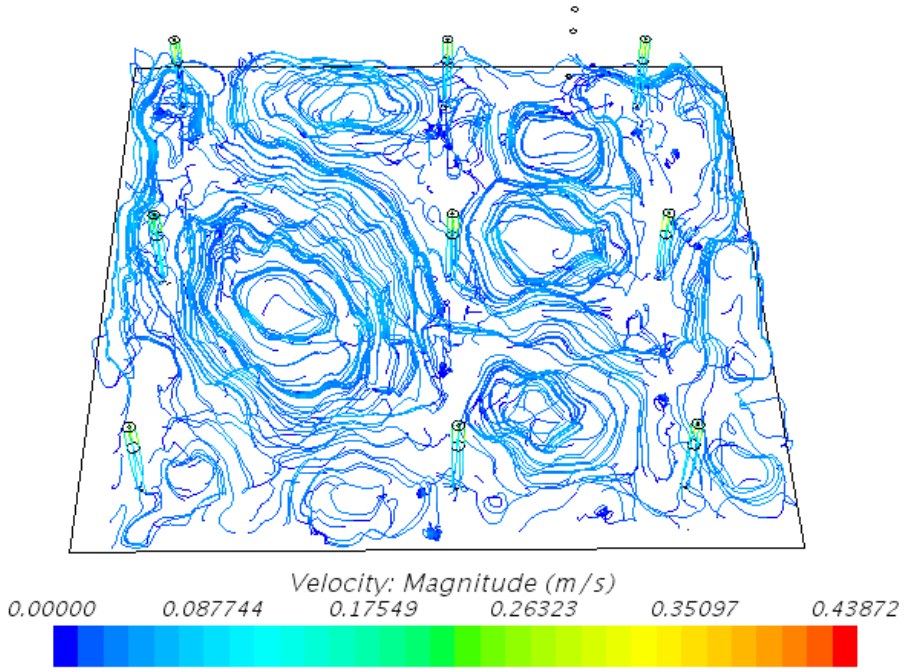

Figure 4.43 Streamlines when changing gaseous purge percentages, isometric view

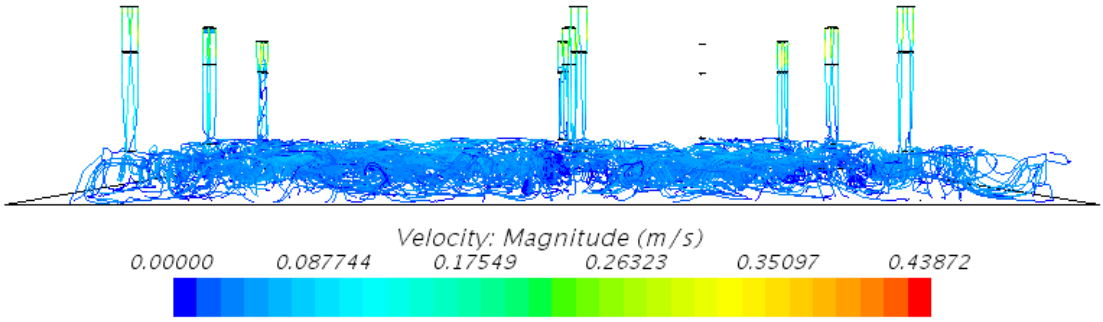

Figure 4.44 Streamlines when changing gaseous purge percentages, side view

In this arrangement, there is a nine times more mass flow through the areas that are creating impurities. This causes almost all of the impurities out of the ullage before they would have a change to propagate throughout the ullage. In addition, areas where the temperature is the highest, and therefore where the impurities are being created in the highest concentrations are extremely close to the gas exits. Finally, the areas where the impurities are being created are on average 83 kelvin colder due to the high mass flow rate of the cold gas, decreasing the total amount of impurities being created even further. For these reasons, the total amount of impurities in the ullage is extremely low.

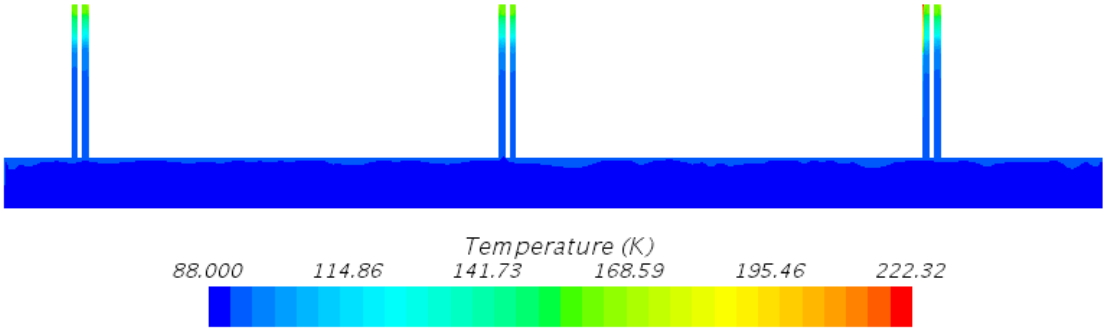

Figure 4.45 Significantly lower temperatures reduce total impurities in the ullage

The total mass of impurities in the simulation when these outgassing percentages are used is 0.0025 grams. It is important to take note that this is based off of the simplified geometry, using nine penetrations instead of more than forty which may or may not be sealed and may or may not be impurity sources. It is also important to note that while researchers think that they know where the impurities are entering the cryostat, they could enter from sources that are not considered here.

One benefit of using the variable inlet was found when comparing the residuals of the variable inlet solution to the constant inlet solution. Figure 4.46 shows the residuals for the variable inlet solution while Figure 4.47 shows the residuals for the constant inlet solution.

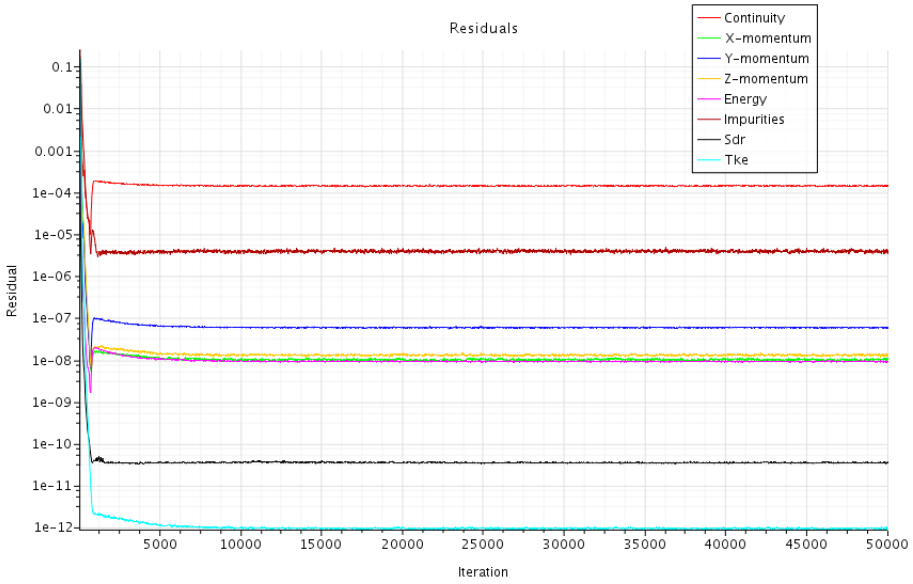

Figure 4.46 Residuals for the variable inlet solution of the ullage

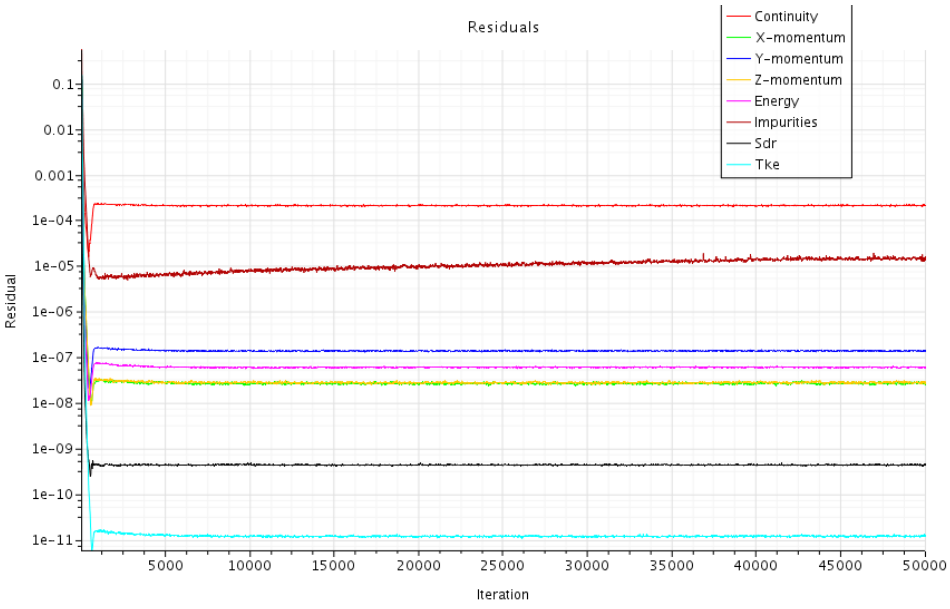

Figure 4.47 Residuals for the constant inlet solution of the ullage

While both of these solutions were run to 50,000 iterations due to assumptions made about convergence time, only the constant inlet simulation really needed to iterate that many times. The variable inlet solution appears to converge after only 10,000 iterations. The significantly smaller number of iterations requires far less resources to reach convergence.

5. CONCLUSSIONS AND FUTURE WORK

5.1 Conclusions

The best boundary conditions for accurate temperature profiles for the ProtoDUNE single-phase detector are a slip shear specification at the surface and a constant surface temperature.

Natural convection accounts for a majority of flow so temperature profiles remain largely unchanged whether liquid argon is being pumped into the cryostat or not.

Pumps and natural convection keep the level of impurity in the cryostat consistent. This consistency leads to even electron lifetimes in the cryostat, eliminating possible sources of error in neutrino detection.

Including a solid insulation model in the simulations gives a more accurate solution for the heat entering the cryostat than assuming an evenly distributed heat flux. Using these numbers, SDSU was able to confirm expected argon gas purge rates and real gas purge rates on the ullage.

Millikelvin accuracy gives confidence that these CFD techniques can be employed on future projects.

Using the heat flux of the liquid simulation as a reference for the amount of gas entering the cryostat creates a more accurate solution and allows the solution to converge more quickly.

5.2 Future Work

Future work should be done on how the electronics of the detector change temperature and cause different flows. Resistances in wires and electrical components

could cause localized heat differences that have the possibility with interfering with temperature profiles on the static and dynamic temperature probes.

The FAR detector is being designed with results from the ProtoDUNE single-phase detector. CFD has proven to be a useful tool in the design of neutrino detectors and should be implemented earlier in the design process to make well informed design decisions.

Doing CFD analysis on the ProtoDUNE dual phase detector would allow us to validate our simulation techniques on a similar detector with similar hardware and geometry without being identical.

Increased complexity on the ullage feedthroughs as well as a better understanding of the sources of impurities would allow for a better impurity simulation on the ullage. DUNE researchers could also confirm the results of the 11% per chimney solution by changing the purge ratios and watching to see if impurities drop in the cryostat. It is assumed that some, if not all, of the impurities come from the ullage, so greatly reducing the amount of impurities by purging gas more evenly across feedthroughs would result in lower impurity levels in the detector.

6. BIBLIOGRAPHY

Brown, G. (2008). From back-room curiosity to mainstream design tool: a short history of CFD modelling at Alcoa World Alumina. *Asia-Pacific Journal of Chemical Engineering*, 119-123.

Cervera, A., & Seong, I. (2018). *ProtoDUNE Single-Phase Sensor Locations*.

Choi, S., Lee, W., & Kim, H. (2017). Numerical analysis of convective flow and thermal stratification in a cryogenic storage tank. *Numerical Heat Transfer*, 402-422.

Collaboration, Tdune. (2017). *The Single-Phase ProtoDUNE Technical Design Reprot.*

Combest, D., Ramachandran, P., & Dudukovic, M. (1996). On the Gradient Diffusion Hypothesis and Passive Scalar Transport in Turbulent Flows. *American Chemical Society Journals*, 8817-8823.

Fermi National Accelerator Laboratory. (2018). *Neutrino Detectors*. Retrieved from Deep Underground Neutrino Experiment: http://www.dunescience.org/neutrino-detectors/

Fujii, K. (2005). Progress and future prospects of CFD in aerospace-Wind tunnel and beyond. *Progress in Aerospace Sciences*, 455-470.

Garcia-Peris, M. A. (2019, 01 16). *Temperature Analysis, Short Update, Calibrating When Pumps Are Off.*

Gray, D. D., & Giorgini, A. (1976). The Validity of the Boussinesq Approximation for Liquids and Gases. *International Journal of Heat and Mass Transfer*, 545-551.

Grayson, G., Lopez, A., Chandler, F., Hastings, L., & Tucker, S. (2006). *Cryogenic Tank Modeling for the Saturn AS-203 Experiment.* Sacramento, CA: NASA Center for AeroSpace Information.

Hanna, K. (2015, March 26). *Mentor*. Retrieved from CFD Breaks the $Billion Barrier!: https://blogs.mentor.com/khanna/blog/2015/03/26/cfd-breaks-the-billion-barrier/

Ho, S., & Rahman, M. (2008). Three-dimensional analysis for liquid hydrogen in a cryogenic storage tank with heat pipe-pump system. *Cryogenics*, 31-41.

Juretić, F., & Gosman, A. (2010). Error Analysis of the Finite-Volume Method with Respect to Mesh Type. *Numerical Heat Transfer*, 414-439.

Kurbatskii, A. (2004). The Difference in Turbulent Diffusion between the Active and Passive Scalars in a Thermally Stably Stratified Medium. *High Temperature*, 79-87.

Liu, Y., Olewski, T., & Vechot, L. (2015). Modeling of a cryogenic liquid pool boiling by CFD simulation. *Journal of Loss Prevention in the Process Industries*, 125-134.

Misra, D., & Sarkar, A. (1997). Finite element analysis of conjugate natural convection in a square enclosure with a conducting vertical wall. *Computer Methods in Applied Mechanics and Engineering*, 205-219.

Omri, M., & Galanis, N. (2007). Numerical Analysis of Turbulent Buoyant Flows in Enclosures: Influence of Grid and Boundary Conditions. *International Journal of Thermal Sciences*, 727-738.

Prasad, B. (2003). ASME Fluids Engineering Divion Newsletter, 2003: Summer., (pp. 6-7).

Propst, A. (2017). *CFD Analysis Methods for Systems Driven by Natural Convection.* Brookings, SD: South Dakota State University.

Resolved Analytcs. (2018, September 26). *Comparing CFD Software*. Retrieved from Resolved Analytics: https://www.resolvedanalytics.com/theflux/comparing-cfd-software

Siemens. (2018). *STAR-CCM+ User Guide.* Munich: Siemens.

U.S. Department of Commerce National Bureau of Standards. (1969). *Thermodynamic Properties of Argon From the Trimple Point to 300 K At Pressures to 1000 Atmospheres*. Washington, D.C.: U.S. Government Printing Office.

Voirin, E. (2016). *ProtoDUNE Ullage Space CFD Model Simulated with and without cooling nozzles*. Washington D.C.: Fermi Research Alliance.

Zhang, Z., Zhai, Z. Q., Zhang, W., & Chen, Q. Y. (2007). Evaluation of various turbulence models in predicting airflow and turbulence in enclosed environments by CFD: Part 2-comparison with experimental data from literature. *Hvac& Research, 13*(6), 871-886.